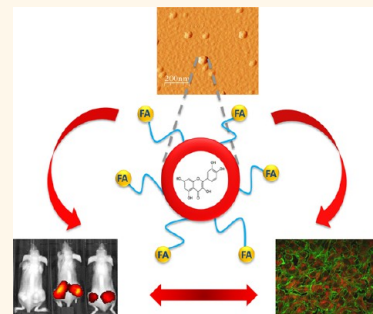


Polyethylene Glycol Conjugated Polymeric Nanocapsules for Targeted Delivery of Quercetin to Folate-Expressing Cancer Cells *in Vitro* and *in Vivo*

Riham I. El-Gogary,^{†,§} Noelia Rubio,^{§,†} Julie Tzu-Wen Wang,^{§,†} Wafa' T. Al-Jamal,[§] Maxime Bourgognon,[§] Houmam Kafa,[§] Muniba Naeem,[§] Rebecca Klippstein,[§] Vincenzo Abbate,[§] Frédéric Leroux,[‡] Sara Bals,[‡] Gustaaf Van Tendeloo,[‡] Amany O. Kamel,[†] Gehanne A. S. Awad,[†] Nahed D. Mortada,[†] and Khuloud T. Al-Jamal^{§,*}

[†]Ain Shams University, Department of Pharmaceutics and Industrial Pharmacy Faculty of Pharmacy, Ain Shams University, Khalifa El-Maamon Street, Abbasiya Square, Cairo 11566, Egypt, [‡]EMAT, University of Antwerp, Groenenborgerlaan 171, 2020 Antwerp, Belgium, and [§]Institute of Pharmaceutical Science, King's College London, Franklin-Wilkins Building, 150 Stamford Street, London SE1 9NH, United Kingdom. ^{†,‡}Equal contribution.

ABSTRACT In this work we describe the formulation and characterization of chemically modified polymeric nanocapsules incorporating the anticancer drug, quercetin, for the passive and active targeting to tumors. Folic acid was conjugated to poly(lactide-co-glycolide) (PLGA) polymer to facilitate active targeting to cancer cells. Two different methods for the conjugation of PLGA to folic acid were employed utilizing polyethylene glycol (PEG) as a spacer. Characterization of the conjugates was performed using FTIR and ¹H NMR studies. The PEG and folic acid content was independent of the conjugation methodology employed. PEGylation has shown to reduce the size of the nanocapsule; moreover, zeta-potential was shown to be polymer-type dependent. Comparative studies on the cytotoxicity and cellular uptake of the different formulations by HeLa cells, in the presence and absence of excess folic acid, were carried out using MTT assay and Confocal Laser Scanning Microscopy, respectively. Both results confirmed the selective uptake and cytotoxicity of the folic acid targeted nanocapsules to the folate enriched cancer cells in a folate-dependent manner. Finally, the passive tumor accumulation and the active targeting of the nanocapsules to folate-expressing cells were confirmed upon intravenous administration in HeLa or IGROV-1 tumor-bearing mice. The developed nanocapsules provide a system for targeted delivery of a range of hydrophobic anticancer drugs *in vivo*.



KEYWORDS: PLGA · active targeting · hydrophobic drugs · HeLa cells · *in vitro* · confocal microscopy · AFM · nanomedicine · anticancer

Polymeric nanocapsules (NCs) are sub-micronic nanoparticulate carriers composed of an oily core surrounded by a polymeric shell with lipophilic and/or hydrophilic surfactants assembled at the interface.¹ The main advantages of polymeric NCs include the possibility of loading high amount of water insoluble drug molecules into the oil core, their physicochemical stability, and protection against enzymatic degradation due to the presence of the polymeric wall. It is proposed that NCs could also reduce toxicity and improve the pharmacokinetic profile of hydrophobic drugs.^{2,3} It is thought that NCs with appropriate size and surface properties can accumulate in

solid tumors by the enhanced permeability and retention (EPR) effect, and thus, can exhibit enhanced anticancer activity and reduced side effects. In addition, NCs offer advantages of ease of modification of their surface properties *via* chemical modification of its constituting polymers. It is postulated that appropriate modification of the surface of these carriers may result in a more efficient targeting of the bioactives. However, little work has been done concerning the surface modification of polymeric oil-cored NCs especially those involving covalent linkage of moieties for the passive or active targeting to tumor tissues and for imaging purposes. Covalent linkage of the

* Address correspondence to khuloud.al-jamal@kcl.ac.uk.

Received for review October 3, 2013 and accepted January 7, 2014.

Published online January 07, 2014
10.1021/nn405155b

© 2014 American Chemical Society

surface polymer to polyethylene glycol (PEG) can provide protection of the nanocapsules against recognition by opsonins thus allowing prolonged blood circulation profile which is a prerequisite to achieve the EPR effect and then active targeting of tumor cells. PEGylated PLGA copolymers have shown extended blood circulation times and reduced liver accumulation in mice.^{1,2,4,5} Covalent conjugation of specific ligands such as folic acid (FA) could provide active targeting and enhanced uptake of the nanocapsules by tumor cells overexpressing folate receptors while sparing healthy tissues thus increasing tumor cells specificity, improving drug efficacy and reducing its associated side effects.

Quercetin (3, 3', 4, 5, 7-pentahydroxyflavone) is a naturally occurring flavonoid found in plants.⁶ It has been recently extensively investigated for its biological activities, such as anti-inflammatory, antioxidant, hepatoprotective activities, antitumor and antiproliferative effects on a wide range of human cancer cell lines.^{6–9} The mechanism of its antitumor and antiproliferative effect was demonstrated to occur *via* glycolysis and macromolecules synthesis inhibition in addition to inhibition of enzymes such as matrixmetalloproteinases (MMPs), NaKATPase, protein kinase C, tyrosine kinases, and pp60 kinase.^{10–14} Moreover, it was reported to inhibit heat shock protein 70 (HSP70) synthesis and expression in tumor cells. Quercetin could also potentiate the action of some cytotoxic agents such as cisplatin.^{6,14} As a result, quercetin was considered as a promising candidate for clinical trials. An obstacle toward the introduction of quercetin in clinical trials is its extreme water insolubility. Many attempts have been made by researchers to facilitate its administration by using dimethyl sulfoxide (DMSO) as a vehicle.¹⁴ However, DMSO safety is questionable as it carries risks of vasoconstriction and neurological toxicity, in addition to liver and kidneys toxicity.^{6,8} In another approach, a water-soluble derivative of quercetin has been synthesized, but a bioavailability of only 20% was obtained.¹⁵ Various techniques have also been used to improve quercetin's aqueous solubility *via* complexation with cyclodextrins¹⁶ for example. In addition, liposomal formulations have previously been reported.⁶ Nevertheless, the use of cyclodextrins was reported to have a risk of nephrotoxicity, while stability problems during storage were experienced in case of liposomes.¹⁷ Therefore, there is still an unmet need for formulating a safe, stable, and efficient delivery system that is capable of solubilizing quercetin to allow its administration *in vivo*.⁸

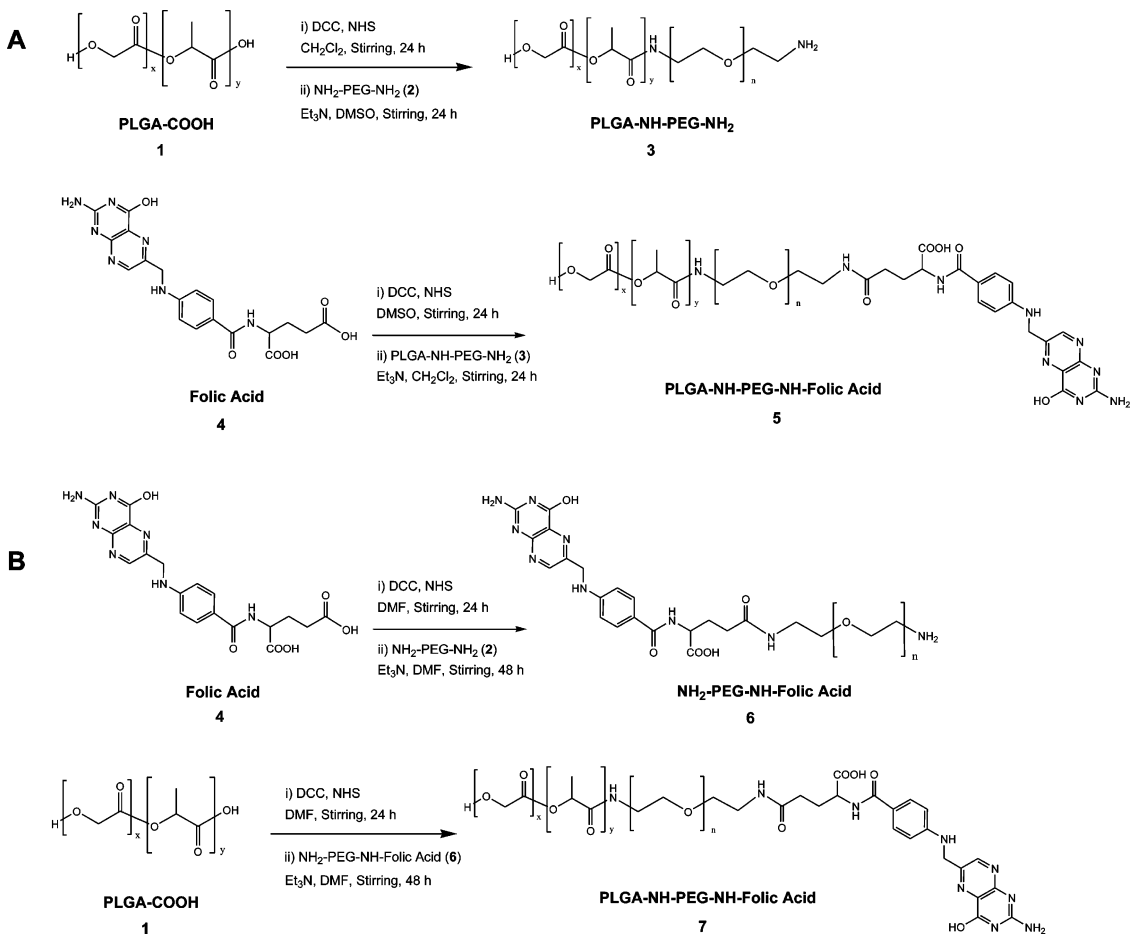
In this work, various types of modified PLGA derivatives were synthesized with the aim of preparation of passively and actively targeted NCs. The lipid soluble drug quercetin was encapsulated in the oil-cored polymeric NCs and the physicochemical characterization of these formulations was performed.

The cytotoxicity profile, targeting, and cellular uptake properties of PEGylated NCs (FA-targeted or non-FA-targeted) were tested in folate expressing HeLa cell line. The passive accumulation of both types of NCs in HeLa and IGROV-1 xenografts was shown *in vivo* after intravenous administration in tumor-bearing mice. The FA-targeted NCs demonstrated active targeting in addition to their passive accumulation in folate-enriched tumors *in vivo*.

RESULTS

Confirmation of Conjugates Formation by FTIR and ¹H NMR.

In this study, we aimed to synthesize PEGylated FA-targeted PLGA conjugates which can be used to formulate PEGylated FA-targeted NCs capable of encapsulating quercetin for subsequent cancer targeting and delivery. Two methods for the synthesis of PEGylated FA-targeted PLGA conjugates were performed, as schematically presented in Scheme 1. In the first method, PLGA-COOH was reacted with excess PEG bis-amine to form PLGA-NH-PEG-NH₂ conjugate (conjugate **3**). Excess PEG bis-amine was used to prevent formation of PLGA-NH-PEG-NH-PLGA dimers as the second COOH was needed to conjugate FA (targeting moiety). The excess unreacted PEG bis-amine was removed by dialysis against deionized water while the excess dicyclohexylcarbodiimide (DCC), N-hydroxysuccinimide (NHS) and dicyclohexylurea (DCU) were removed by precipitation of the polymer in diethyl ether where the byproducts remain soluble. Characterization of PLGA-NH-PEG-NH₂ (Conjugates **3**) was performed by FT-IR and ¹H NMR. The presence of free NH₂ group in the synthesized polymer was confirmed by Ninhydrin/Kaiser test (data not shown). FT-IR chart (Figure 1, inset) confirmed the conjugation of PEG to the activated PLGA-COOH through the appearance of vibration frequencies at 1621 cm⁻¹ (amide C=O) and 1563 cm⁻¹ (N–H bond) that were absent in PLGA-COOH and PEG bis-amine charts (Figure S1A,B). ¹H NMR also confirmed the presence of PLGA and PEG protons on the NMR spectra (Figure 1A).¹⁸ The appearance of peaks at 1.6, 4.8, and 5.2 ppm in ¹H NMR (Figure 1) charts were related to the CH₃, CH, and CH₂ protons of PLGA, respectively. The peak at 3.6 ppm accounted for the CH₂ protons of PEG blocks. PLGA-PEG polymer was washed with a solution of 0.1 M HCl in order to confirm that the FT-IR was reflecting the covalent amide bond and was not an artifact of electrostatic interaction. The obtained solid was studied by FT-IR and the spectrum was compared with the physical mixture of PLGA + PEG and PLGA-PEG polymer before washing with HCl. As shown in Figure S2, amide bands are observed at 1550 and 1650 cm⁻¹ before and after washing with acidic solution. However, for the physical mixture, these bands were weaker and shifted to lower wavenumbers confirming the formation of an amide linkage between PLGA-COOH and PEG bis amine.



Scheme 1. Synthesis of the modified and unmodified conjugates using 2 synthetic approaches. Conjugate 3 (PLGA_{18kDa}-PEG_{3.5kDa}-NH₂) contained no targeting moiety (FA), while the modified conjugates 5 and 7 (PLGA_{18kDa}-PEG_{3.5kDa}-NH-FA) contained equal amount of PEG_{3.5kDa} and FA.

Conjugate 3 was further reacted with FA (1:5), compound 4, yielding PLGA-NH-PEG-NH-FA (conjugate 5).^{18–20} Removal of unreacted excess FA was performed by Gel Permeation Chromatography (GPC) using SephadexLH-20 column where unreacted FA got trapped in the column while the polymer (PLGA-NH-PEG-NH-FA) eluted the column by size exclusion using DMF as a mobile phase. FTIR and ¹H NMR are shown in Figure 1.

In the second preparation method, PEG bis-amine was first reacted with FA (1:1). H₂N-PEG-NH-FA (conjugate 6) was purified by elution through SP-SephadexC25 column.²¹ The presence of monofunctionalized H₂N-PEG-NH-FA was confirmed by Ninhydrin test (data not shown). Conjugation of FA to PEG bis-amine was confirmed by FT-IR (Figure S1C) through the appearance of vibration frequencies at 1621 cm^{-1} (amide C=O) and 1563 cm^{-1} (N–H bond) and the decrease in the amine bond vibration at 3400 nm indicating coupling of one of the amine terminals. Conjugate 6 was then reacted with the activated form of PLGA-COOH resulting in the formation of PLGA-NH-PEG-NH-FA (conjugate 7). Conjugate 7 was characterized by FT-IR and ¹H NMR (Figure 1C). FT-IR showed the

appearance of vibration frequencies at 1621 cm^{-1} (amide C=O) and 1563 cm^{-1} (N–H bond). ¹H NMR indicated the presence of PLGA protons (1.6, 4.8, and 5.2 ppm) in addition to PEG protons (3.6 ppm) in conjugate 7. FT-IR and ¹H NMR of the precursors PLGA-COOH (compound 1), PEG bis-amine (compound 2) are shown in Figure S1. Kaiser test (Ninhydrin) was used to detect the presence of free amino group in conjugates 3 and 6.^{22,23} We obtained free amines values of 47.5 and 270 $\mu\text{mol/g}$ polymer for conjugates 3 and 6, respectively. The latter has a higher value as it consists only of PEG which is smaller in MW than the PLGA-PEG so higher free amine content per gram was obtained. The conjugates were then freeze-dried. Combination of FT-IR, ¹H NMR and UV-vis spectrophotometry altogether confirmed the chemical conjugation and formation of required conjugates.

Quantification of PEG and FA Contents in the Conjugates. To ensure that all PEGylated conjugates contained equivalent amount of PEG, the PEG content in conjugates 3, 5, and 7 was measured using BaCl_2/I_2 colorimetric assay as described in Supporting Information.^{24,25} The three conjugates were found to have similar PEG content ranging from 14.8 to 16% of the total polymer

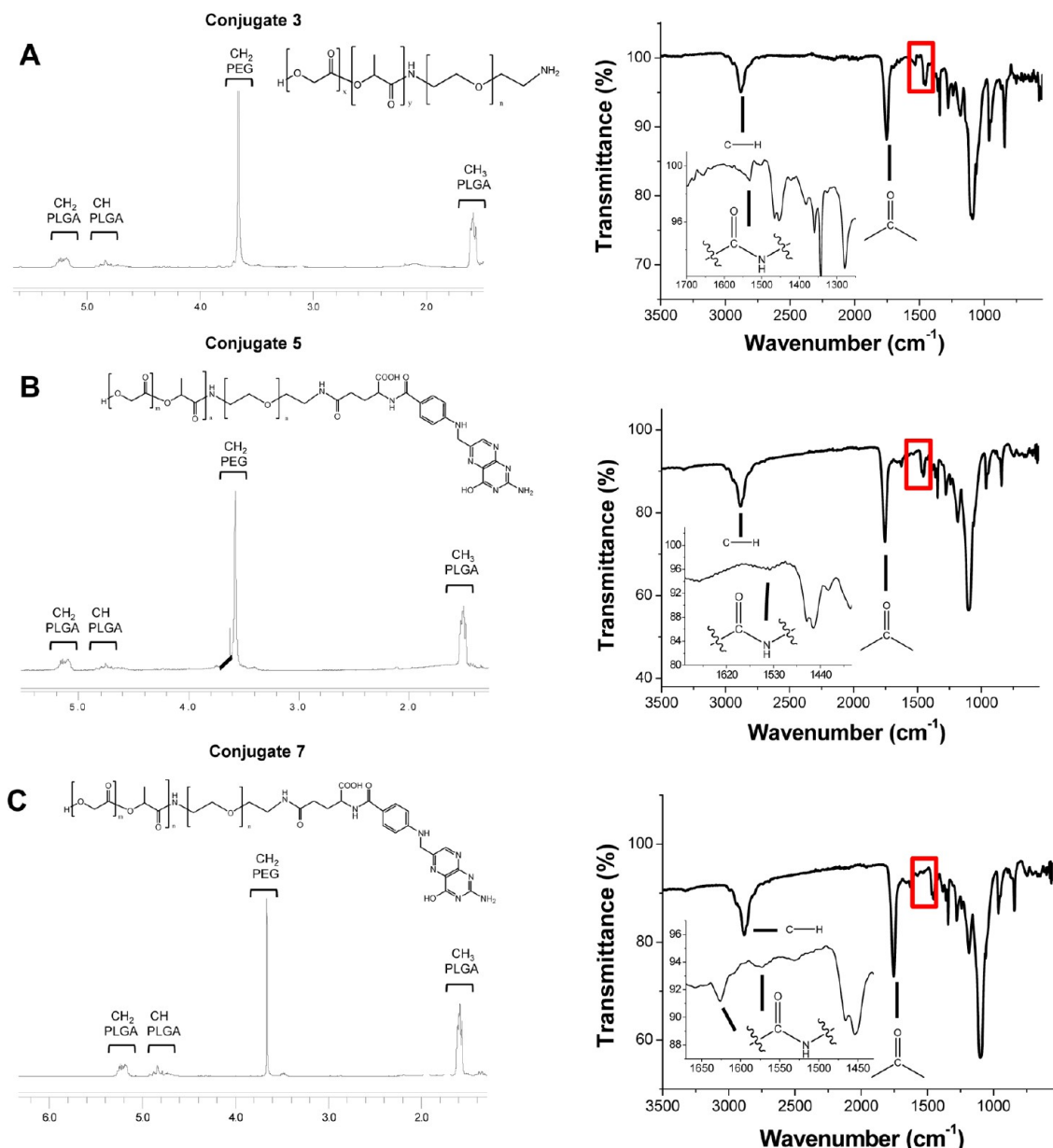


Figure 1. Characterization of the synthesized conjugates by NMR and FT-IR. ^1H NMR spectra (CDCl_3) and FT-IR spectra (ATR mode) of (A) conjugates 3 ($\text{PLGA}_{18\text{kDa}}\text{-PEG}_{3.5\text{kDa}}\text{-NH}_2$) and (B and C) conjugates 5 and 7 ($\text{PLGA}_{18\text{kDa}}\text{-PEG}_{3.5\text{kDa}}\text{-NH-FA}$), respectively. Insets show enlargement of amide region ($1700\text{--}1200\text{ cm}^{-1}$).

TABLE 1. Characterization of PLGA Conjugates

polymer	PEG content ^a (w/w %)	folic acid content ^b ($\mu\text{mol/g}$)
Conjugate 3	14.81 ± 4.36	-
Conjugate 5	15.22 ± 4.49	47.50 ± 2.89
Conjugate 7	16.00 ± 1.87	41.50 ± 12.02

^a Determined by BaCl_2/I_2 colorimetric assay. ^b Determined by spectrophotometric assay.

weight. The amount of FA in conjugates 5 and 7 after purification was measured spectrophotometrically at 365 nm (Table 1). The two conjugates were found to have similar FA content of $41\text{--}47.5\text{ }\mu\text{mol FA/g polymer}$. This further confirmed that both conjugation

strategies were able to incorporate equal amount of PEG and FA into the conjugates. A summary of PEG and FA contents in the conjugates is presented in Table 1.

Formulation and Physicochemical Characterization of the Nanocapsules. After synthesis and confirmation of the structures of the conjugates, NCs were formulated from their respective polymers. Formulations prepared include (a) the non-PEGylated, non-FA targeted, NC 1; (b) PEGylated, non-FA targeted, NC 3; (c) PEGylated, FA-targeted, NC 5 (synthetic method A) and (d) PEGylated, FA-targeted, NC 7 (synthetic method B). All formulations were prepared using the interfacial deposition method.²⁶ Particle size, polydispersity index, zeta-potential measurements and drug encapsulation

TABLE 2. Physicochemical Characterization of PLGA Based nanocapsules

formulation	particle size \pm SD ^a (nm)	PDI \pm SD	zeta-potential \pm SD (mV)	encapsulation efficiency ^b (EE%)
nc 1	153.0 \pm 4.3	0.11 \pm 0.01	-46.2 \pm 1.5	98.10 \pm 0.28
nc 3	143.1 \pm 1.7	0.13 \pm 0.01	-32.9 \pm 1.8	99.00 \pm 0.42
nc 5	155.0 \pm 1.2	0.19 \pm 0.01	-40.0 \pm 0.9	97.8 \pm 0.14
nc 7	155.2 \pm 1.6	0.19 \pm 0.01	-43.4 \pm 3.0	97.85 \pm 0.21

^a Measured by dynamic light scattering. ^b Calculated as a percentage of the drug added determined by spectrophotometry.

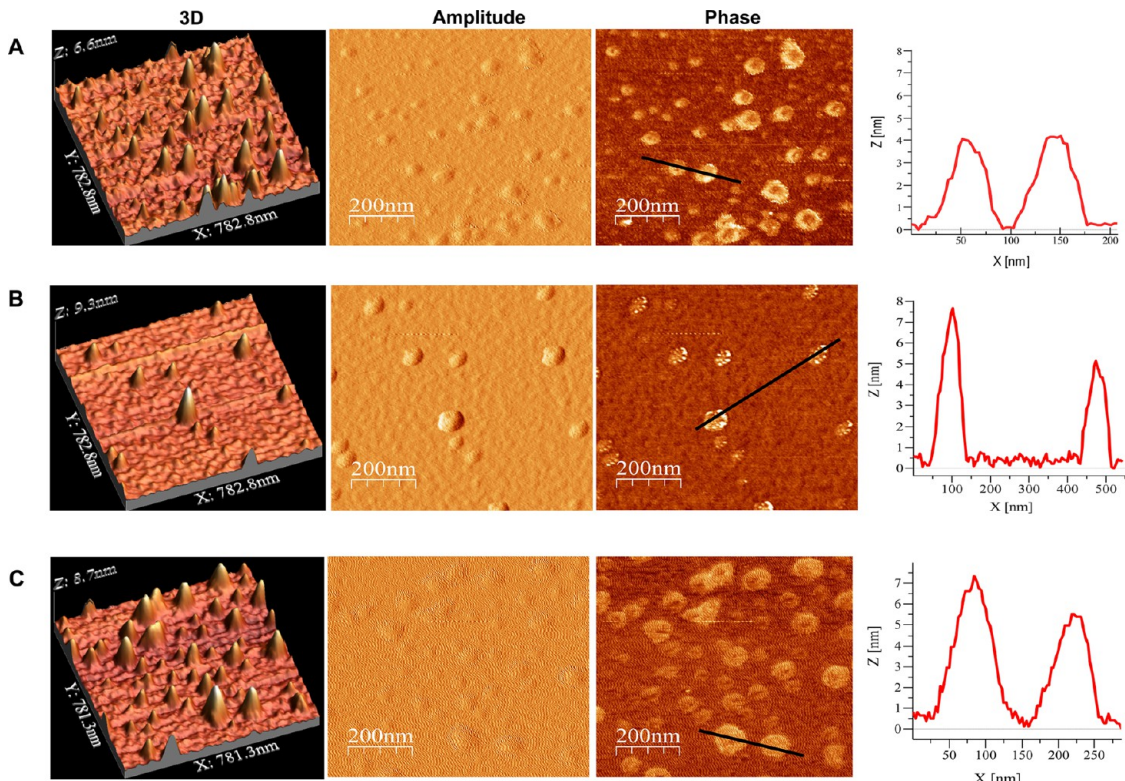


Figure 2. AFM measurements of the different NCs prepared. The 3D, amplitude, phase image and cross-section analysis of NC 1, NC 3, and NC 5. The different NC formulations were filtrated through a Sephadex PD-10 column and dispersions of 100 μ g/mL were prepared. Tapping mode AFM analysis (TM-AFM) on the poly lysine coated mica substrates were carried out in air at 25 $^{\circ}$ C. The average sizes obtained were similar for all the preparations. The average height values obtained from cross section were less than 6 nm for the different nanocapsule prepared.

efficiency of the different formulations are described in Table 2. The hydrodynamic size of all formulations ranged between 143 and 155 nm. A significant decrease ($p < 0.05$) in average size was observed in case of the PEGylated non FA targeted compared to the non-PEGylated formulations by dynamic light scattering. The polydispersity index was lower than 0.2 in all formulations conferring the homogeneity of all the preparations.

The negative zeta-potential imparted by the PLGA polymer and lecithin (Table 2) was slightly masked by the presence of PEG chains decreasing zeta-potential significantly from -46.2 to -32.9 ($p < 0.001$).^{27,28} The presence of FA increased the values of zeta-potential again to -40.0 and -43.4 mV in NCs 5 and 7, respectively, presumably due to presence of free carboxylic groups of FA ($p < 0.001$). Similar size and zeta-potential of NCs 5 and 7 was obtained further confirming a

similar behavior of both polymers synthesized using two chemical approaches. Since NC 5 and NC 7 exhibited similar physicochemical characteristics, the former was used in the rest of *in vitro* investigations.

The encapsulation efficiency (EE%) of the drug in NCs, shown in Table 2, ranged from 97 to 99% due to the high solubility of the drug in the oil core and its very low aqueous solubility. The encapsulation of quercetin in NCs neither significantly affected the mean diameter nor the zeta-potential values of the nanocapsules (data not shown). Removal of unencapsulated drug was carried out using Nanosep membrane filtration method.²⁹

AFM was used to elucidate the structural characteristics of the nanocapsules formulated in this work. AFM allows the measurement of the size of the nanocapsules in a partially dried state. A droplet of poly lysine was deposited on freshly cleaved mica surface for

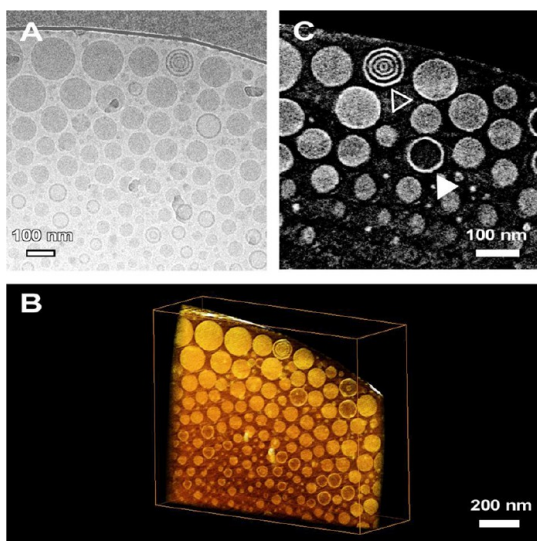


Figure 3. Cryo-transmission electron microscopy. (A) A 2D projection image which is part of the tilt series of an image that was acquired at cryo conditions. A 3D visualization of the outcome of the 3D reconstruction is presented in (B). A slice through the 3D reconstructed volume is presented in (C) which enables one to investigate the inner structure of the capsules; most of them are filled, but also hollow NCs (indicated by the white arrow) and other of multilamellar vesicular nature were observed (indicated by the open arrow).

2 min and then dried with air, followed by the deposition of a droplet of the nanocapsule sample. The different formulations were studied in air, using tapping-mode AFM. The nanocapsules showed a homogeneous distribution in size, height and in three-dimensional images shown in Figure 2 and Figure S3. The average sizes obtained were 56.55 ± 8.35 nm ($n = 40$, NC 1), 60.47 ± 8.6 nm ($n = 40$, NC 3) and 59.03 ± 8.79 nm ($n = 40$, NC 5). The sizes obtained for the different NC preparations were similar, however, the height was remarkably reduced as obtained from the cross-section analysis for all the formulations: NC 1 (3.5 ± 0.37 nm), NC 3 (5.28 ± 1.22 nm) and NC 5 (4.44 ± 1.45 nm). The presence of a halo at the edge of the NC in the AFM images is supportive of the hypothesis that the polymeric shell surrounds the oily core.

The NCs were also imaged by electron tomography in order to investigate their 3D morphology. To study the nanocapsules in their original hydrated state, these experiments were carried out under cryo conditions using a sample in which the NCs are embedded in a layer of vitreous ice. During electron tomography, a tilt series of 2D images was acquired and combined into a 3D reconstruction of the sample. The results for sample NC 3 are presented in Figure 3, showing a 2D projection image from the tilt series in Figure 3A. A visualization of the 3D reconstruction is presented in Figure 3B and movies are provided in the Supporting Information (Movies S1 and S2). NCs with spherical morphology and different diameters can be clearly observed. Since the spherical morphology is confirmed, the average sizes

from 2D images were measured. The average diameters were found to be 115 ± 48 nm ($n = 85$, NC 1) and 84 ± 55 nm ($n = 85$, NC 3). These measurements were in agreement with the AFM data but were smaller than hydrodynamic diameters obtained by dynamic light scattering (Table 2). Electron tomography also enables one to investigate the inner structure of the NCs. A slice through the 3D reconstruction is presented in Figure 3C. Interestingly, empty capsules were found as indicated by the white arrow in Figure 3C and some of the NC exhibited a multilamellar vesicular nature of liposomes (indicated by the open arrow in Figure 3C).

Shelf Life Stability and Drug Release Studies. It was shown that the three formulations: NC 1, NC 3 and NC 5 exhibited similar release profile in the presence or absence of serum up to 1 h (Figure 4). In case of serum absence, a total of 40–50% of the drug was released over the first 24 h with no significant differences seen among the three formulations. In the presence of serum, approximately the same release values were obtained up to 8 h incubation period for the formulations NC 5 ($54\% \pm 1.33$) and NC 3 ($51\% \pm 0.76$). NC 1, however, showed faster release profile ($72\% \pm 0.32$) than the PEGylated NCs ($p < 0.001$). Such results indicated a higher stability of PEGylated nanocapsules (NC 3 and NC 5) compared to the non-PEGylated preparation (NC 1) in serum presence. The difference remained significant ($p < 0.001$) after 24 h incubation with serum where NC 1 exhibited the highest release rate ($87\% \pm 3.05$) followed by NC 5 ($73\% \pm 2.03$) then NC 3 ($79\% \pm 0.67$). On the other hand, DMSO control showed rapid release of the drug into the dialysate with more than 50% of the drug being released within the first half an hour, as expected (Figure 4).

In terms of shelf life stability, no significant changes in hydrodynamic sizes and zeta-potential values were observed in all NCs formulations even after 3 months of storage at 4°C , as shown in Table S1. The optimum shelf life stability and high EE% of these NCs in addition to the optimum particles size of both modified and unmodified PLGA formulations were very encouraging that further studies were carried out to determine the candidacy of these NCs formulations for targeting and delivery of the drug quercetin to folate-enriched cancer cells *in vitro*.

Cellular Cytotoxicity Studies in Cancer Cell Lines *in Vitro*. MTT assay was used to screen the *in vitro* cytotoxicity of the quercetin in various types of cancerous cell lines: HeLa cells (cervical-tumor-derived cell line), the CT26 (murine colon carcinoma), C6 (rat glioma) and B16F10 (murine melanoma). Cells were incubated with a range of drug concentrations (0.001 – $100 \mu\text{M}$) for 48 h. Interestingly, various cell lines responded differently to drug toxicity with HeLa and CT26 cells being most sensitive to the drug toxicity (Figure S4). Percentage

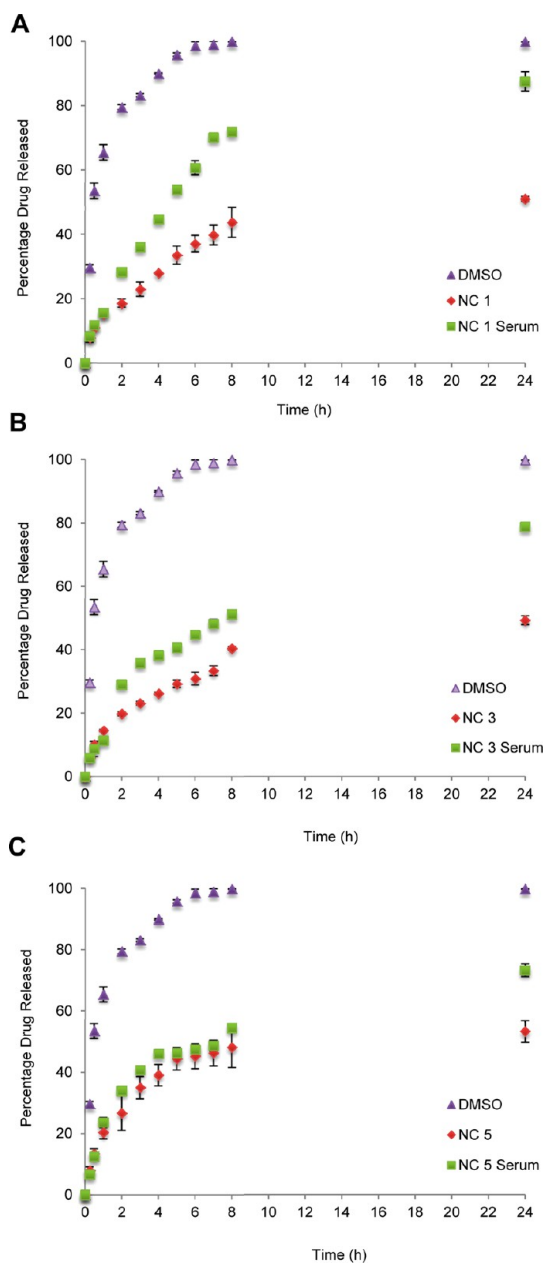


Figure 4. Release profile of quercetin from different NC formulations. NCs were dialyzed in 1% w/v Tween 80 in phosphate buffered saline (PBS), pH 7.4, in the presence and absence of serum of (A) NC 1, (B) NC 3, and (C) NC 5. Drug concentration in the dialysate was assessed by measuring the absorbance at 350 nm. To assess serum stability, rat serum was added to the NC at 33.3% final serum concentration. A control experiment was set up concurrently in which the same amount of quercetin was dissolved in DMSO and dialyzed for comparison.

cell viabilities obtained were $81.70\% \pm 5.75$ (C6), $56.09\% \pm 8.20$ (B16F10), $47.08\% \pm 8.73$ (CT26) and $43.99\% \pm 3.95$ (HeLa) (at $10 \mu\text{M}$ after 48 h). At the highest concentration tested ($100 \mu\text{M}$), no significant differences in cytotoxicity were obtained between the three cell lines, CT26, B16F10 and HeLa with cell viability in the range of 11–19% was obtained. CT26 and HeLa cells were selected to test the cytotoxicity of

the nontargeted and targeted NC formulations as a negative and positive cell lines for FA receptor, respectively. The level of folic acid expression in these cell lines was validated by quantitative PCR (Figure S5).

The cytotoxicity of different quercetin formulations was tested in both CT26 and HeLa cell lines after 48 h of incubation in serum containing media. Formulations tested were the following: (a) the drug alone dissolved in DMSO; (b) the non-PEGylated, non-FA targeted, NC 1; (c) PEGylated, non-FA targeted, NC 3; and (d) PEGylated, FA-targeted, NC 5. Figure S6 showed that quercetin encapsulation in the NCs did not compromise the drug toxicity in both cell lines and that no significant difference was shown between the various formulations at all concentrations tested.

HeLa cell line has been reported in the literature as a model of folate-expressing cells therefore was selected for testing the cytotoxicity of the drug-loaded NCs *in vitro* (Figure S5).^{30–32} For this purpose, HeLa cells were seeded in FA-free RPMI media for 24 h and then were incubated with different types of NCs formulations in (a) FA-containing media ($200 \mu\text{M}$ FA) or (b) FA-free RPMI media, both at $10 \mu\text{M}$ quercetin for 24 h. Formulations tested were the following: (a) the drug alone dissolved in DMSO; (b) the non-PEGylated, non-FA targeted, NC 1; (c) PEGylated, non-FA targeted, NC 3; and (d) PEGylated, FA-targeted, NC 5. The concentration and time point were selected in this study as the drug showed to be *moderately* toxic (40–60%) under these conditions thus any improvement in cytotoxicity can be clearly demonstrated. The concentration of FA supplemented to the media was determined by testing a range of FA concentrations (1 – $2000 \mu\text{M}$) where FA concentrations higher than $1000 \mu\text{M}$ (Figure S4B) showed intrinsic cytotoxicity to cells thus FA concentration of $200 \mu\text{M}$ was used in competitive uptake inhibition studies. Expectedly, in the absence of FA, significant differences were obtained between the targeted and nontargeted NC formulations tested (Figure 5). The PEGylated, FA-targeted NC 5 exhibited the least cell viability (56.63%) compared to the drug alone (84.36%), the non-PEGylated non-FA targeted NC 1 (83.22%) and the PEGylated non-FA targeted NC 3 (81.27%) treated cells. In the presence of excess folic acid, no difference in cytotoxicity profile was shown among all the formulations. Interestingly, the murine Colon Cancer CT26 cells, used as a negative cell line in this study, did not show a statistically significant difference in the cytotoxicity when treated with both types of NCs in the presence or absence of FA (Figure S7). This result further confirmed the selectivity of formulated NCs in targeting folic acid receptor.

Folate Targeted NCs Demonstrated Enhanced Uptake in HeLa Cells Using Spectrofluorimetry. To understand the mechanisms behind enhanced cytotoxicity of FA-targeted NCs 5 in comparison to other formulations, another experiment was carried out where the NCs was fluorescently

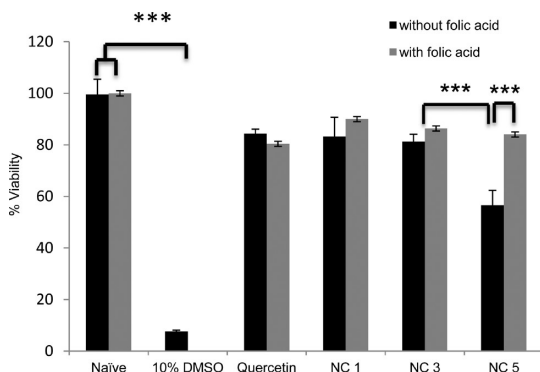


Figure 5. Cell viability of HeLa cells in the presence of quercetin nanoformulations in the presence and absence of FA. HeLa cells were seeded in 96-well plates (6K per well) overnight in FA free media then incubated with the free quercetin or its nanoformulations at 10 μ M drug concentration for another 24 h using FA-free media (black solid bars) or FA-supplemented media (at 200 μ M FA) (gray solid bars) as an incubation media. Nanoformulations tested were NC 1 (non-PEGylated NC), NC 3 (PEGylated NC), NC 5 (FA-conjugated PEGylated NC). Cell viability was assessed using MTT assay. Cell viability was expressed as a percentage of control untreated cells (mean \pm SD; $n = 5$). HeLa cells exhibited exceptionally lower cell viability when incubated with NC 5 in the absence of FA in the incubation media which was reversed when excess FA was present. *** $p < 0.001$.

labeled to quantify the uptake of the NCs inside cells. Fluorescently labeled formulations [(a) the non-PEGylated, non-FA targeted, NC 1; (b) PEGylated, non-FA targeted, NC 3 and (c) PEGylated, FA-targeted, NC 5] were prepared by incorporating the lipid soluble fluorescent dye, 1,1'-dioctadecyl-3,3',3'-tetramethylindocarbocyanine perchlorate (DiI) in the oil core of the NCs. Dye concentration was optimized so that uptake of NCs quantities as low as 0.1% of the treatment dose can be detected in cell lysates. HeLa cells were seeded in folate free RPMI media overnight. On the day of treatments, cells were incubated with drug-free NCs (10 μ g/mL) in FA-free or FA-containing media (200 μ M FA), for 1 or 4 h. Cells were lysed and total fluorescence signals were measured using a plate reader. Confirming the results of MTT assay, Figure 6 showed enhanced cellular uptake of NC 5 compared to NC 3 at both 1 h and 4 h in FA-free medium ($p < 0.001$). The uptake of NC 5 into the cells significantly decreased in the presence of excess FA ($p < 0.001$). This suggested that excess FA in the medium prevented NC 5 from being taken up by the cells through competitive binding to folate receptors present on the surface of HeLa cells. It is worth mentioning that the same results were obtained at a higher NCs concentration (100 μ g/mL) (Figure S8), indicating the selectivity of the targeted NCs was preserved even at higher NCs concentration.

Folate Targeted NCs Demonstrated Intracellular Delivery in HeLa Cells by Confocal Laser Scanning Microscopy (CLSM). To confirm intracellular delivery of the NCs, HeLa cells were treated under the same conditions used in fluorescence measurements. Cells were fixed and stained for F-actin

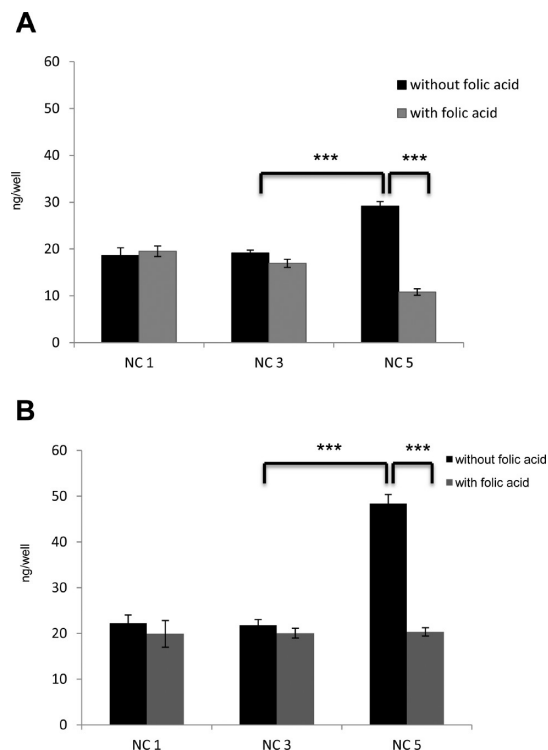


Figure 6. Quantitative measurement of cellular uptake of NCs in HeLa cells by spectrofluorimetry. HeLa cells were seeded in 96-well plates (6K per well) overnight in FA free media then incubated with DiI-labeled drug-free nanoformulations at 10 μ g/mL NC concentration for for 1 h (A) or 4 h (B) using FA-free media (black solid bars) or FA-supplemented media (at 200 μ M FA) (gray solid bars) as incubation media. Nanoformulations tested were NC 1 (non-PEGylated NC), NC 3 (PEGylated NC), and NC 5 (FA-conjugated PEGylated NC). At the end of incubation period, cell were rinsed, lysed, and measured for fluorescence in a FLUOstar OPTIMA plate reader at 590 nm emission wavelength. Only NC 5 (FA-conjugated PEGylated NC) showed significantly higher uptake in HeLa cells in the absence of FA. Higher uptake was observed after 4 h compared to 1 h. No difference in uptake was obtained between all the formulations in the presence of excess FA. Results are represented as mean % uptake and mean \pm SD ($n = 5$). *** $p < 0.001$.

(green) and examined by CLSM. Uptake of the NCs was confirmed by the presence of red signals (Figure 7 and Figure S9). Results have confirmed the enhanced cellular uptake of NC 5 in HeLa cells in the absence of FA. No red fluorescence signals (indicating no uptake) were detected in HeLa cells cultured in high-FA medium. Such results together with total fluorescence measurements indicated that selective uptake and active targeting of FA-targeted NCs in cancer cells overexpressing folate receptors have been achieved.

In Vivo and ex Vivo Tumor Uptake Studies. *In Vivo* tumor accumulation of NC 3 and NC 5 was assessed using DiI-labeled NCs in two folate enriched tumor xenograft models. Whole body imaging was carried out up to 24 h after injection followed by imaging of excised tissues. Tumor uptake of NC 3 and NC 5 was clearly observed in both tumor xenografts when imaged from the dorsal view (Figure 8A). In contrast to those mice

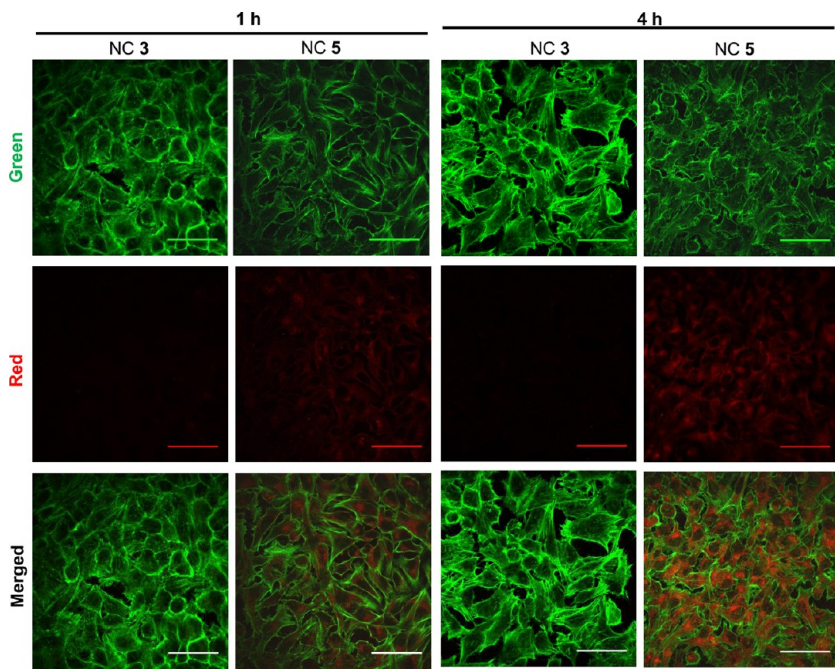


Figure 7. Cellular uptake of NCs by confocal laser scanning microscopy (CLSM). CLSM images of FA-deprived HeLa cells incubated with Dil-labeled NC 3 (PEGylated NC) and NC 5 (FA-conjugated PEGylated NC) for 1 h (left panels) or 4 h (right panels). Cells were deprived of FA for overnight period and during incubation with the NCs. At the end of incubation period, cell were rinsed, fixed, permeabilized, and subsequently stained with Alexa Fluor 488 phalloidin (green color, F-actin). NC uptake was indicated by red fluorescence (Dil) inside the cells. Only NC 5 (FA-conjugated PEGylated NC) showed positive uptake in HeLa cells in the absence of FA. Signals were more intense after 4 h compared to 1 h. CLSM images were captured using a Nikon Eclipse Ti Inverted confocal microscope (63 \times lens). Scale bar is 50 μ m.

injected with NCs, no fluorescence signals were detected from naïve mice. The fluorescence image of excised organs is shown in Figure 8B where the highest fluorescence intensities were measured from the tumors compared to other organs. Fluorescence intensities from each organ were further quantified and the results were shown in Figure 8C and Figure S10A. Taking into account the weights of the samples, slightly higher fluorescence signals per gram of tissue were calculated from lung than tumors. Lower values were obtained from the rest of the tissues which was expected from the fluorescence image shown in Figure 8B. Figure 8D depicts the tumor uptake of NC 3 and NC 5 in both types of xenografts. Although brighter signals were captured from IGROV-1 tumors (Figure 8B and Figure S10B), comparable fluorescence signals per gram of tumor were measured from either formulation in both tumor models. Organs to tumor ratios were plotted in Figure S10C. Confocal imaging of frozen HeLa tumor sections also confirmed the tumor uptake of both formulations (Figure 8E) but showed a slightly different distribution patterns with NC 3 showed more homogeneous distribution while NC 5 showed more granular patterns hence brighter signals inside tumor cells.

DISCUSSION

Quercetin is a hydrophobic drug which is extremely water insoluble. Several attempts have been made to

improve quercetin's water solubility including preparation of its nanoformulations for the purpose of its application as an anticancer or an antioxidant agent. Nanocarriers described so far for this purpose include liposomes,⁶ solid lipid nanoparticles (SLN),^{33,34} micro-emulsion,³⁵ and nanoparticles.^{36,37} Few reports described the preparation of PLGA- and PLA-based nanoparticles for quercetin delivery.^{36–39} To our knowledge, only one type of sustained release polymeric lipid-core NCs encapsulating quercetin (as antioxidant agent) has been described with no active targeting to specific tissue approach being proposed.⁴⁰ The previously reported formulation was based on poly(ϵ -caprolactone) (PCL) polymer (hydrophilic shell) and medium-chain triglyceride and sorbitan monostearate as liquid and solid lipophilic components dispersed in the core of the NC with reported hydrodynamic size of 212 nm. The only stealth nanoformulations reported and tested *in vivo* for quercetin delivery as an anticancer drug agent for parental use were based on a liposomal preparation.^{6,41} Another study reported the formulation of PEGylated PLA nanoparticles encapsulating quantum dots (QDs) (for imaging) and quercetin (as an anticancer drug) for drug delivery to HepG2 cells but this study was only done *in vitro* without *in vivo* validation of the system.⁴² Another study by Wang *et al.* formulated lipid based assemblies of PEG2000-DPSE-coated quercetin nanoparticles and proved its enhanced anticancer effect through

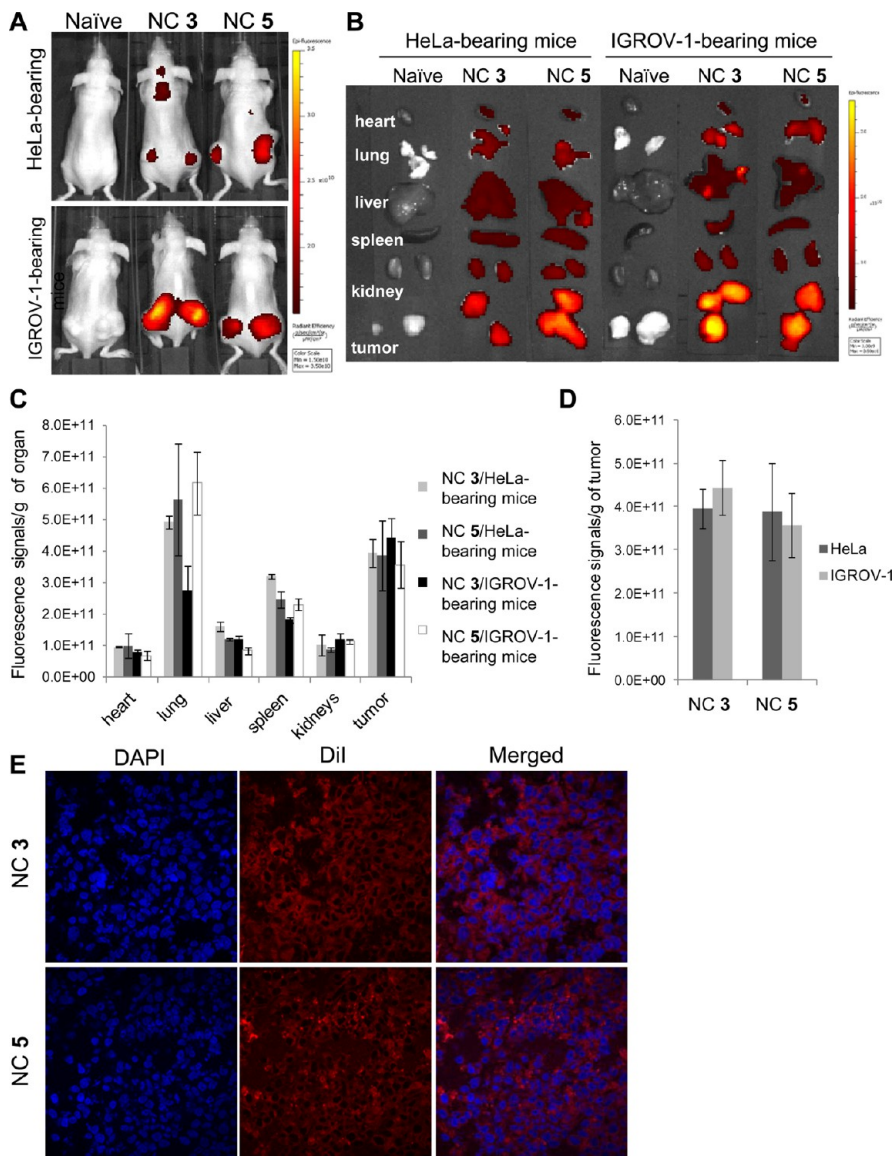


Figure 8. *In vivo* and *ex vivo* imaging of DiR labeled NCs in FR + tumor-bearing mice. (A) Representative whole body imaging of HeLa or IGROV-1 tumor-bearing mice at 24 h post iv injection of DiR labeled NC 3 or NC 5. (B) Representative fluorescence images of NCs in excised organs and tumors. Fluorescence signals refer to radiant efficiency ($(p/s)/(\mu W/cm^2)$). (C) CLSM images of frozen sections of HeLa tumors excised at 24 h after iv injection of Dil-labeled NCs. The red color maps the distribution of Dil-labeled NCs and the blue color represents DAPI stained nuclei. Both types of NCs appeared to be present in the tumor mass with more intense signals observed for NC 5 injected tumors.

induced programmed cell death on C6 glioma cells *in vitro*.⁴³ None of these two studies, however, has incorporated the active targeting delivery approach.

Few groups reported the formulation of PEGylated PLGA and PLA polymeric NCs, however, not for the purpose of quercetin delivery. Mosqueira *et al.*⁴ formulated PLA-PEG NCs containing different PEG densities and proved that some PEG chain lengths (20 kDa) prevented protein adsorption and reduced interaction with macrophages, and showed optimal blood circulation time *in vivo* using nontumor bearing mice model.¹ Neckel *et al.* reported the formulation of PLA and PLA-PEG NCs for encapsulation of

campotethin (CPT) and confirmed that PLA-PEG NCs were more effective in treating lung metastases (B16F10 model) than the non-PEGylated NCs.²⁷

Active targeting aims at delivering drug to the desired site of action while minimizing its exposure to nontarget organs. Active targeting of nanocarriers can potentially increase the efficacy and reduce the toxicity of the therapeutic agents.²⁰ FA has been widely used to actively target nanocarriers for anticancer drugs delivery to tumors due to its small size, low cost, high tumor tissue specificity, nonimmunogenic nature, ease of conjugation and stability unlike biological ligands.¹⁸ In this study, FA-PEG-PLGA NCs were

designed to target folate receptors (FR) overexpressed on tumor cells, in this case, cervical and ovarian cancer. To our knowledge, this is the first report on the preparation of FA-targeted stealth PLGA NCs encapsulating quercetin for cancer targeting and therapy for *in vivo* use.

Two methods for the synthesis of folate modified polymers used in NCs formulations were employed. The two methods were found to incorporate similar amounts of PEG and FA in the conjugates. The amount of FA loading obtained in our study was $41-47\text{ }\mu\text{mol/g}$ of polymer following purification by FA precipitation and chromatographic techniques to ensure the absence of any free FA in the final conjugates. In a previous study by Boddu *et al.*²⁰ formulating PLGA-PEG-FA nanoparticles ($\sim 200\text{ nm}$ hydrodynamic diameter) using single emulsion solvent evaporation (SESE) method to deliver doxorubicin, various methods for FA conjugation to the polymer were utilized and the conjugation yield ranged from 8.15 to $28\text{ }\mu\text{mol FA/g}$ of polymer upon optimization of the chemical conjugation strategies. If FA conjugation to polymer is to be expressed as "tagging ratio" or the percentage of polymer chains that contained FA, the results in conjugates **5** and **7** have tagging ratios of $\sim 100\%$ and $\sim 89\%$, respectively. Boddu *et al.*²⁰ reported FA tagging ratio of 52% as they reported a value of $8.15\text{ }\mu\text{mol FA/g}$ of polymer (MW of their polymer was 40 kDa). At their highest, a tagging ratio of 100% was achieved; however, taking into consideration that the MW of their polymer (40K) is higher than what we report here (18K), it can be concluded that more FA per gram of polymer was obtained in our study compared to Boddu *et al.*²⁰ which is an advantageous property when considering targeting properties of the NCs *in vivo*. Furthermore, the FA yield in our study was independent of the synthetic approaches used (Scheme 1) and higher than the best yield obtained in Boddu *et al.*²⁰

In this study, quercetin NCs were successfully prepared with an optimal size range for passive accumulation of NCs in tumors by EPR effect. Polymer modification did not affect NCs hydrodynamic size and EE% but affected zeta-potential measurements. A slight but significant reduction in average size was observed upon PEGylation. A similar effect was observed by Mosqueira *et al.*¹ and Pereira *et al.*² upon comparing the average size of PLA and PLA-PEG NCs where PEGylation of PLA NCs reduced their size from 218 ± 52 and 282 ± 24 to 200 ± 51 and $216 \pm 36\text{ nm}$ in both studies, respectively. This could be attributed to the hydrophilic properties of PEG that imparted amphiphilic property to the polymer thus reducing the interfacial tension between the aqueous and organic phase.⁴⁴

Both non-PEGylated and PEGylated NCs exhibited negative zeta-potential due to the presence of terminal carboxylic groups in the polymer.^{18,20} However, a

reduction in the negativity of the zeta-potential of the NCs was observed upon PEGylation which can be attributed to the conversion of COOH groups to amide linkages upon conjugation to PEG-bis amine and the presence of PEG free amine terminals. The fact that zeta-potential values varied among the different NCs types indicated that the polymer orientation was more likely to be out-facing rather than inward-facing which is expected due to hydrophilicity of PEG chains. Similarly, Mosqueira *et al.*⁴ formulated PLA NCs using Miglyol oil, epikuron 170 and poloxamer as surfactants and obtained a zeta-potential value of $-47.7 \pm 0.5\text{ mV}$ which decreased to -35.5 to -5.5 mV when PEGylated. Ameller *et al.*⁴⁵ formulated PLGA NCs of the pure antiestrogen RU 58668 using Soy phosphatidylcholine Lipoid S75 as a lipophilic surfactant and miglyol as an oil core. Similarly, the zeta-potential of the unloaded and loaded PLGA NCs was found to be -53.4 ± 0.5 and $-45.2 \pm 1.9\text{ mV}$, respectively. The use of PEGylated PLGA polymer did not cause a significant reduction in zeta-potential values in their study presumably due to the higher amount of lipophilic surfactant and the high MW of PLGA polymer used. Interestingly, herein, an increase in the negative values in the zeta-potential was observed upon FA conjugation to the PEG chains. This could be attributed to the presence of another free COOH available in FA structure. This result is in line with that obtained by Boddu *et al.*²⁰ However, the reduction in overall negativity upon PEGylation in their study was attributed to the presence of the positively charged amine groups in FA but no PEG-PLGA NPs (without FA) were employed in their study. It is clear from our results that the reduction in zeta-potential of the PEGylated NCs was related to the shielding of COOH groups by PEG and not due to presence of FA molecules as explained by Boddu.²⁰

AFM and cryo-TEM have been used to elucidate the structural characteristics of the NCs formulated in this work. AFM allows the measurement of the size of the NCs in a partially dried state. The sizes and heights obtained for the different NCs preparations were similar but smaller than measurements obtained by dynamic lights scattering (measuring the hydrodynamic diameter of the NCs). The difference in size measurements obtained by the two different techniques could be due to a possible NCs flattening on mica as has been previously reported.⁴⁶ The phase images indicate the presence of a halo in the periphery of the NCs presumably due to the presence of the polymeric wall surrounding the oily core. Such observation corroborates the presence of two different materials forming the NCs. Cryo-TEM allows direct investigation of colloids in the vitrified, frozen-hydrated state, *i.e.*, very close to their native state, to obtain information about the internal structure of the colloidal particles. In this study, cryo-EM showed clearly the presence of

polymeric shell surrounding the oil core. Other studies by Kuntsche *et al.*⁴⁷ and Mosqueira *et al.*⁴⁸ also reported very few liposomal structures in addition to the capsular nature of the nanoparticles/nanocapsules, due to the presence of surfactants in the dispersion. Such structures are similar to what we obtained in our study (Figure 3).

The main hindrance for the clinical use of quercetin is its extreme water insolubility, so the high drug encapsulation efficiency ranging from 97 to 99% achieved solved the problem of its parenteral administration. There was an almost 50-fold increase in drug water solubilization obtained ($\sim 2500 \mu\text{M}$) compared to only $50 \mu\text{M}$ (intrinsic solubility) reported for the free drug.⁴⁹ No significant difference in EE% among the various formulations was reported suggesting that EE% is a function of the volume of the oil core and also the type of oil and not directly dependent on the polymeric shell type. These results were in line with those obtained by Lu *et al.*³¹ and Nie *et al.*³² where encapsulation efficiency was independent of the type of polymer used. Another major advantage of this formulation is the excellent shelf life stability which is a problem encountered with liposomes. As hypothesized, the presence of the negatively charged soybean lecithin in addition to the PEGylated polymeric shell around the oil core may have stabilized the NCs for relatively such a long period of time. The relatively high negative zeta-potential values could have also prevented the collision between the NCs.⁵⁰ Despite the high EE% reported previously for the PEGylated liposomal formulation,⁶ the nanoformulation reported in this study offers, in addition to the high loading and formulation stability, the ease in chemical modification allowing for incorporation of stealth properties and active targeting without compromising the size, the drug loading, or the stability of the NCs.

It is important that the NCs are able to release the drug when needed. In some of the previous reports, ethanol was used in the dialysis media which was avoided in this report to avoid destabilization of the polymeric shell. Quercetin release from SLN under sink conditions in 65:35 ethanol/water (release medium) showed $\sim 90\%$ drug release during the first 24 h³³ which was also shown by Dhawan *et al.*³⁴ where $\sim 60\text{--}90\%$ of the drug was released within 24 h using phosphate buffered saline (pH 7.4) and methanol (80:20, v/v) as release media. Faster drug release was seen from PLA nanoparticles exhibiting a burst release effect ($\sim 45\%$ and 87.6% after 0.5 and 96 h, respectively).³⁶ Gang *et al.*⁴¹ reported 66% and 85% release after 12 h from non-PEGylated and PEGylated liposomes, respectively. Herein, we have shown that approximately 50% release after 24 h in all the formulations which is in line with Dhawan *et al.*³⁴ and Wang *et al.*⁴² studies carried out in PBS. Significantly lower amounts ($p < 0.001$) of quercetin were released from PEGylated NCs (NC 3 and

NC 5) than the non-PEGylated ones (NC 1) after 8 and 24 h in the presence of serum in the dissolution medium. The better stability of stealth NCs in the presence of serum compared to the non-PEGylated NCs could be attributed to the presence of PEG that decreases the adsorption of serum proteins which destabilizes the NCs. Similar findings have been reported by Mosqueira *et al.*⁵¹ where their PLA-PEG NCs retained the lipophilic antimalarial drug better than non-PEGylated NCs in plasma-containing media. Pereira *et al.*² have also reported a slower release of $^{99\text{m}}\text{Tc-HMPAO}$ complexes from PEGylated PLA NCs compared to the non-PEGylated ones.

Quercetin exhibited similar cytotoxicity profiles in both CT26 and HeLa cells *in vitro* where the incubation of cells with quercetin at 10 and $100 \mu\text{M}$ led to less than 40% and 15% viability (at 48 h of incubation), respectively. A mechanistic study by Priyadarsini *et al.*⁵² studying the antiproliferative effect of quercetin on HeLa cells showed $\sim 50\%$ cell viability at $80 \mu\text{M}$ by MTT assay after 24 h incubation. Taking into account that the latter study was carried out using MTT assay after 24 and not 48 h as was the case in our study, we concluded that both studies are in good agreement. Furthermore, it was observed that encapsulating quercetin in the different NCs did not alter the cytotoxic effect of the drug. This result was in agreement with a previous study which found that quercetin loaded PEGylated liposomes (Q-PEGL) exerted similar cytotoxicity profile on CT26 to that of the free drug at all time points tested with 60% inhibition at $33 \mu\text{M}$ after 48 h, almost equal to values we report in this study.⁶ On the contrary, Goniotaki *et al.*⁵³ reported a reduction in quercetin cytotoxicity in SF268 cells (central nervous system), H460 (non-small cell lung) and MCF7 (breast) cell lines when incorporated in egg phosphatidylcholine (EPC) liposomes. This could be attributed to the large size of liposomes obtained by Goniotaki *et al.* (414.1 ± 12.6), compared to the ones prepared by Yuan *et al.*⁶ (130 ± 20), which could have affected the degree of nanocarrier uptake by the cells.

HeLa cells were selected as a model cell line for comparative uptake and toxicity studies. HeLa cells over-express folate receptors (FRs) in response to special need for FA to maintain their growth and proliferation rate. These FRs usually reside on the outer surface of cell membranes surface thus recognize and bind FA and FA targeted NPs.³¹ FA-targeted PEGylated NCs showed higher cytotoxicity compared to the free drug and other NCs in folate-free medium, while similar cytotoxicity profile was obtained in presence of excess FA. Such results confirmed the original hypothesis that FA-targeted NCs are internalized into folate-enriched cells *via* FRs and, thus, can be used to target selective cancer cell populations.

To study the uptake profile of different NCs formulations into HeLa cells, NCs were labeled with the fluorescent probe (Dil) by its incorporation in the oil core of NCs taking

advantage of the lipophilicity of Dil and its solubility in the oil core of NCs. In case of *in vivo* studies, Dil was exchanged with DiR which absorbs light in the near-infrared (NIR) region, thus allowing for better tissue penetration and signal-to-noise ratio. The lipophilic nature of Dil and DiR prevents their release from the NCs as has been shown by Petersen *et al.* where only a small amount of the highly lipophilic Dil dye was transferred after a period of weeks.⁵⁴ This confirms that tracking the NCs uptake by this labeling method is indeed reliable. Cellular uptake studies (CLSM and spectrofluorimetry) correlated well with the cytotoxicity assay (at 24 h) where folate-PEGylated NCs exhibited the highest uptake in HeLa cells in comparison to other nontargeted formulations after 1 and 4 h incubation in folate-free medium. Higher uptake was observed after 4 h incubation compared to that of 1 h. Such results indicated that the enhanced cytotoxicity of the targeted NCs was directly proportional to the enhanced uptake into HeLa cells (in absence of FA in the media). This was further confirmed by the fact that the addition of excess FA to the culture media diminished both cellular uptake and toxicity of the targeted NCs with no significant differences obtained between the drug containing treatments group. PEG chain is expected to act as a spacer between PLGA copolymer and FA so that the binding of FA to its receptor is not obstructed.

Several folate-targeting strategies have been previously proposed including folate-targeted liposomes,^{55,56} folate-targeted polymeric nanospheres,^{18,20,57} folate-targeted PEGylated PLGA NPs,^{20,57,58} folate-targeted PLGA-PEG-FA micelles¹⁹ and folate-targeted nanohydrogel.⁵⁹

To our knowledge, no chemically modified FA-targeted PEGylated polymeric NCs with a core–shell structure has been prepared and tested previously. The closest to our system was described by Rata-Aguilar *et al.*⁶⁰ in which FA–chitosan conjugate was utilized to physically coat the preformed oil–lecithin NCs with folic acid. The previously reported strategy exhibited colloidal instability in cell culture medium due to the medium salinity, while in our case, the system was stable and withstood the biological environment as demonstrated by ability to target folate enriched cells *in vitro* and *in vivo*.

The work was extended to target FR positive tumors *in vivo*. This is a challenging task as it is necessary that the NCs withstand the biological environments and remain stable in the blood with sufficient blood circulation time so that an enhanced permeation and retention effect can be obtained prior to active targeting. Studies by Gabizon *et al.*⁵⁵ and Xiang *et al.*⁵⁶

reported that folate targeted liposomes (FTLs) were cleared faster than nontargeted pegylated ones (NTLs) from the bloodstream. This was attributed to uptake of the targeted liposomes by FR in the liver. However, no significant difference was found neither in tumor cell uptake in both M109-FR or KB solid tumors nor in the therapeutic efficiency of doxorubicin.

In our study, *in vivo* optical imaging demonstrated a very clear tumor delineation of both NC **3** and NC **5** using the two FR+ tumor xenografts: HeLa and IGROV-1. Similar tumor accumulation (%ID/g tumor) was obtained for both NCs suggesting that initial tumor accumulation has occurred mainly due to the EPR effect. However, an altered intratumoral distribution was detected by CLSM with better association of NC **5** with cancer cells, indicating that FA may play a role in selective uptake of the targeted NCs by the FR+ cells *in vivo*. This finding correlates well with the *in vitro* results thus suggesting the selectivity of the prepared NCs *in vitro* and *in vivo*.

CONCLUSION

The chemical conjugation and formation of conjugates **3**, **5**, and **7** was confirmed by FT-IR and ¹H NMR analyses. All conjugates showed similar and high PEG content (around 14–16%). Moreover, the FA content of conjugates **5** and **7** were found to be similar with tagging ratio close to 100%. AFM and TEM studies confirmed the spherical shape of NCs and the presence of polymer shell around the oil core. Both PEGylated and non-PEGylated NCs showed good shelf life stability and high quercetin EE% in addition to optimal particle sizes. PEGylated NCs were found to be more stable and displayed a slower quercetin release profile in the presence of serum compared to the release profile obtained in PBS. Nanoencapsulated quercetin showed similar cytotoxicity to free quercetin on different cell lines, while FA-conjugated NC **5** enhanced the cell killing as well as the cellular uptake observed in folate-enriched HeLa cells in folate free medium. Reversed results were also obtained using medium containing excess folic acid. Tumor uptake was further demonstrated *in vivo* by live fluorescence imaging of FR+ tumor-bearing mice iv injected with NC **3** or NC **5**. Moreover, NC **5** showed an altered intratumoral distribution and better association with cancer cells in these tumor sections by CLSM. In conclusion, the present PEGylated FA-targeted NC showed enhanced uptake in folate receptor enriched cancer cells *in vitro* and *in vivo* *via* passive- and active-targeting. Future plans will focus on carrying out cancer therapy studies *in vivo*.

EXPERIMENTAL SECTION

Materials and Reagents. Quercetin (HPLC purity >95%), folic acid, dicyclohexylcarbodiimide (DCC), *N*-hydroxysuccinimide

(NHS), anhydrous dimethylformamide (DMF), dialysis tubing (MWCO 2000 Da), SP-Sephadex C-25 resin, 3-(4,5-dimethylthiazol-2-yl)-2,5-diphenyltetrazolium bromide (MTT), 1,1'-dioctadecyl-

3,3,3',3'-tetramethylindocarbocyanine perchlorate (Dil), and Triton-X-100 were purchased from Sigma. 1,1'-Diiodadecyl-3,3,3',3'-tetramethylindocarbocyanine iodide (DiR) was purchased from Biotium, Inc. Sephadex LH-20 was obtained from GE Healthcare. Polyoxyethylene-bis-amine (PEG bis-amine, MW ~3500) was purchased from JENKEM USA. DL-Lactide/glycolide copolymer 75/25 (PLGA-COOH, MW ~18 000) was a gift from Purac Biomaterials. Snake Skin dialysis tubing (MWCO 10 000 Da) was purchased from Thermo-Fisher. Soybean lecithin (Epikuron 140 V) was a kind gift from Cargill Pharmaceuticals. Castor oil, Tween 80, methylene chloride, acetone, absolute ethanol, dimethylsulfoxide (DMSO) and diethyl ether (ultra pure grades) were obtained from Sigma Aldrich. NANOSEP (100 kDa cut off) were obtained from Pall Life Sciences. RPMI-1640 media with and without folic acid, Dulbecco's modified Eagle media, fetal bovine serum (FBS), penicillin/streptomycin, Trypsin/EDTA, phosphate buffered saline (PBS), and Alexa Fluor 488 phalloidin were obtained from Gibco, Invitrogen. Quantifoil R 2/2 grids were obtained from Electron Microscopy Sciences (EMS, Hatfield, PA). Mica sheets (11 mm × 11 mm × 0.15 mm) were used for atomic force microscopy experiments (AFM). Mowiol 4-88, mounting media was from Polysciences; 16% formaldehyde, methanol-free, was from Thermo Scientific Pierce. All reagents were used without further purification.

RNAs were extracted using Tripure (Roche Diagnostics) and reverse transcription was performed using QuantiTect Reverse Transcription Kit (Qiagen Ltd, Manchester, UK). Specific primers were designed using the Probe Design 2.0 software (Roche Diagnostics). Primers were used at 200 nM and were chosen as follows: forward primers for human FOLR1, residues from 173 to 192, 5'-GAGGACAAGTTGCATGAGCA-3'; reverse primers, residues from 224 to 242, 5'-CCTGGCTGGTGGTGGAGA-3'; forward primers for human GAPDH, residues from 83 to 101, 5'-AGCCA-CATCGCTCAGACAC-3'; reverse primers, residues from 130 to 148, 5'-GCCAAATAGCAGACAAATCC-3'. In addition, forward primers for murine FOLR1, residues from 335 to 354 5'-CTTCAACCGGACTGACTTCC-3'; reverse primers, residues from 445 to 464, 5'-CCCGAGTAGCTCTGGACTGA-3'; forward primers for mouse GAPDH, residues from 133 to 155, 5'-GGGTTCTATAATACGGACTGC-3'; reverse primers, residues from 225 to 244, 5'-GGGTTCCATAATACGGACTGC-3'. PCR was conducted at a final concentration of 1× PCR buffer, TaqMan Universal PCR Master Mix, No Amperase (Applied Biosystems, Life Technologies). For each cDNA sample, four unique fluorescently labeled hydrolysis probes (Roche Ltd.) were used to target mouse FOLR, mouse GAPDH, human FOLR, and human GAPDH.

Synthesis of the Conjugates. **Conjugate 3.** PLGA-NH-PEG-NH₂ conjugate **3** was prepared according to the method developed by Yoo and Park, 2004 with some modification.^{18–20} Briefly, PLGA-COOH **1** (700 mg, 0.0412 mmol) and a 4 molar excess of NHS (18.952 mg, 0.1648 mmol) and DCC (33.95 mg, 0.1648 mmol) were dissolved in anhydrous methylene chloride as presented in Scheme 1. The reaction mixture was stirred under nitrogen atmosphere for 24 h at room temperature (RT) for activation of carboxylic group of PLGA-COOH (**1**). The resultant solution was filtered and added dropwise to a mixture of excess of PEG bis-amine (**2**) (721 mg, 0.206 mmol) and triethylamine (57.2 μL, 0.412 mmol) in anhydrous methylene chloride. PLGA-COOH/H₂N-PEG-NH₂ stoichiometric molar ratio was 1:5. The reaction mixture was stirred under nitrogen atmosphere for 24 h at RT. The resultant solution was precipitated by the addition of ice-cold diethyl ether to remove dicyclohexylurea byproduct, unreacted NHS and DCC. The precipitated product, PLGA-NH-PEG-NH₂ **3** was dried, dissolved in DMSO and dialyzed against deionized water for 2 days to remove excess unreacted PEG. Conjugate **3** was then lyophilized and stored at RT until further use. PEG content was assessed colorimetrically upon reaction with barium chloride (in 1 N hydrochloric acid)/iodine solution as described in more details in Supporting Information.

¹H NMR (400 MHz, CDCl₃): δ = 5.05–5.2 (m, CH₂ PLGA), 4.75–4.85 (m, CH PLGA), 3.5–3.6 (m, CH₂ PEG), 1.42–1.6 (m, CH₃ PLGA).

Conjugate 5. PEGylated FA-conjugated PLGA copolymer was synthesized by coupling the PLGA-NH-PEG-NH₂ **3** with an activated FA at PLGA-NH-PEG-NH₂/FA molar ratio of 1:5.

For activation, FA (compound **4**) (51.26 mg, 0.1165 mmol) was dissolved in 8 mL of DMSO along with a 2 molar excess of NHS (16.077 mg, 0.1398 mmol) and DCC (28.659 mg, 0.1398 mmol). The reaction was stirred under nitrogen atmosphere for 24 h at RT. After this period of time, conjugate **3** (500 mg, 0.0233 mmol) was added to the activated FA which was stirred for 24 h at RT. A total of 50 mL of water was added to the mixture to precipitate unreacted FA by centrifugation at 4000 rpm for 5 min. The supernatant containing PLGA-NH-PEG-NH-FA was then dialyzed and freeze-dried. The product was then precipitated in ice-cold diethyl ether to remove dicyclohexylurea byproduct, unreacted DCC, and NHS, filtered and dried. Further removal of free unbound FA was performed by Gel Permeation Chromatography (GPC) using sephadex-LH20 column and DMF as a mobile phase. FA content was assessed spectrophotometrically as described in more details in Supporting Information. The resultant conjugate **5** was stored at RT until further use.

¹H NMR (400 MHz, CDCl₃): δ = 5.05–5.2 (m, CH₂ PLGA), 4.75–4.85 (m, CH PLGA), 3.5–3.6 (m, CH₂ PEG), 1.42–1.6 (m, CH₃ PLGA).

Conjugate 6. FA **4** (45 mg, 0.102 mmol) was dissolved in 10 mL of anhydrous DMF along with a 1.1 molar excess of NHS (12.5 mg, 0.112 mmol) and DCC (20.62 mg, 0.112 mmol) for FA activation. The reaction was stirred under nitrogen atmosphere for 24 h at RT. After this period of time, PEG bis-amine **2** (347.4 mg, 0.102 mmol) and triethylamine (41 μL, 0.306 mmol) were added to the reaction and the mixture was stirred for 24 h at RT. After this period of time, the solution was placed into MWCO 2000 Da dialysis bag and dialyzed against deionized water and then the product was lyophilized. The solid was dissolved in chloroform and precipitated by addition of diethyl ether to remove dicyclohexylurea byproduct, unreacted NHS and DCC. The yellow solid was dissolved in sodium acetate buffer (0.1 M, pH 4.6), and loaded onto a SP-Sephadex C25 cation-exchanger column and eluted using sodium acetate buffer affording H₂N-PEG-NH-FA conjugate **6** separating it from free FA, unreacted PEG bis-amine and disubstituted PEG. The product was dialyzed (MWCO 2000 Da) against deionized water and lyophilized and stored as a yellow solid.

¹H NMR (400 MHz, CDCl₃): δ = 3.65–3.75 (m, CH₂ folate), 3.5–3.6 (m, CH₂ PEG), 3.38–3.43 (m, CH₂ folate), 2.17–2.19 (m, CH₂ folate), 2.07–2.09 (m, CH₂ folate).

Conjugate 7. For activation, PLGA-COOH **1** (279 mg, 0.016 mmol) was dissolved in 10 mL of anhydrous DMF together with a 8 molar excess of NHS (14.29 mg, 0.128 mmol) and DCC (23.56 mg, 0.128 mmol). The reaction mixture was stirred under nitrogen atmosphere for 24 h at RT. After this period of time, conjugate **6** (310 mg, 0.08 mmol) and triethylamine (33.4 μL, 0.24 mmol) were added (PLGA-COOH/H₂N-PEG-NH-FA stoichiometric molar ratio was 1:5) and the reaction mixture was stirred under nitrogen atmosphere for 48 h at RT. The solution was dialyzed (MWCO 10 000 Da) against deionized water and lyophilized. The obtained product was dissolved in chloroform and precipitated by addition of diethyl ether to remove dicyclohexylurea byproduct, unreacted DCC and NHS, affording conjugate **7** as a pale yellow solid.

¹H NMR (400 MHz, CDCl₃): δ = 5.05–5.2 (m, CH₂ PLGA), 4.75–4.85 (m, CH PLGA), 3.5–3.6 (m, CH₂ PEG), 1.42–1.6 (m, CH₃ PLGA).

Formulation of the NCs. Quercetin polymeric NCs were prepared using the nanoprecipitation technique as described by Fessi *et al.*²⁶ Briefly, polymer (50 mg), castor oil (300 μL), quercetin (5 mg) and soybean lecithin (50 mg) were dissolved in 10 mL of acetone/ethanol (60:40, v/v) mixture. This organic phase was added dropwise into an aqueous phase (20 mL) containing Tween 80 (0.2%) as a hydrophilic surfactant; the mixture was maintained under magnetic stirring in the chemical hood for 1 h to allow for solvent diffusion and formation of nanocapsules. Organic solvents were then eliminated by evaporation under reduced pressure using a Buchi rotavap. The final volume of the colloidal suspension was adjusted to 10 mL.

Determination of Encapsulation Efficiency (EE%). The encapsulation efficiency (EE%) of quercetin loaded NCs was determined by measuring the concentration of the free drug in the nanocapsules suspension. The unencapsulated quercetin was

separated by filtration/centrifugation using NANOSEP centrifuge tube fitted with ultrafilter (MWCO 100 kDa). A definite volume of the nanocapsules suspension was transferred to the upper chamber of the Nanosep and centrifuged at 6000 rpm for 60 min. The amount of free drug in the filtrate was measured using UV-vis spectrophotometer (Model UV-1601 PC; Shimadzu, Kyoto, Japan) by measuring the absorbance at 370 nm as previously described.²⁰ The EE (%) was calculated by $EE\% = (([Drug]_{total} - [Drug]_{free})/[Drug]_{total}) \times 100$. The method was validated by calculating the EE% using size exclusion chromatography with PD10 columns and similar results were obtained.

Size and Zeta-Potential Measurements. Measurement of the average size and zeta-potential of the NCs was performed using dynamic light scattering (DLS) with a Nanosizer ZS series (Malvern Instruments, Southborough, MA). Disposable polystyrene cells and disposable plain folded capillary Zeta cells were used. NC suspensions were diluted in deionized water and measurements were performed at 25 °C. Electrophoretic mobility was used to calculate the zeta-potential using the Helmholtz-Smoluchowski equation. The hydrodynamic size was presented as the average value of 20 runs, with triplicate measurements within each run.

Cryo-Transmission Electron Microscopy (Cryo-TEM). Three microliters of each nanocapsule suspension was applied on freshly plasma-cleaned Quantifoil grids. The grid was blotted once for 2 s and the remaining thin aqueous layer was plunge frozen by immersion in liquid ethane. The grids were transferred to a Gatan 626 cryo-holder (Gatan, Inc., Pleasanton, CA). The grid was analyzed at cryogenic temperatures (<−450 K) using a Tecnai Spirit operated at 120 kV. A tilt series was collected over an angular range of ±70° with a 5° increment in BF-TEM imaging mode using a Gatan 626 cryomicrography holder. A total dose of 120 e/Å² distributed over the series and a defocus of −2 μm were used. 3D reconstruction was carried out using 30 iterations of SIRT (simultaneous iterative reconstruction technique) in FEI Inspect3D.

Atomic Force Microscopy (AFM). The surfaces for AFM analysis were prepared as follows: The different NC formulations were filtrated through a Sephadex PD-10 column and solutions of 100 μg/mL were prepared. Poly lysine polymer was deposited on mica surfaces for 5 min and then flushed with air. Subsequently, NC solutions (NC 1, NC 3 and NC 5) were deposited on mica surfaces for 5 min and flushed with air. Tapping mode AFM analysis (TM-AFM) on the mica substrates was carried out in air at 25 °C using a Bruker Dimension ICON with Scan Assist. The surfaces were imaged with a general purpose tapping tip made by MikroMasch in Estonia (NSC15/no Al, tip radius <10 nm; tip height = 20–25 μm; cone angle <40°; cantilever thickness = 3.5–4.5 μm; cantilever width = 32–28 μm; cantilever length = 120–130 μm; frequency f_0 = 265–400 kHz; force constant k = 20–75 N m^{−1}, VEECO). The statistical analysis of the AFM images was carried out using WSxM v5.0 software.

Release Profile and Serum Stability *in Vitro*. Two milliliters of the each formulation containing 2.5 mg (quercetin) in 10 mL was taken and put into a 10 kDa dialysis bag. The dialysis membrane was dialyzed against 40 mL of 0.1% (w/v) Tween 80 in phosphate buffered saline (PBS), pH 7.4. Release was studied at 37 °C at 250 strokes/min. At predetermined time points, 1.5 mL aliquots were taken and replaced by addition of an equal volume of the dialysate to maintain sink conditions. Drug concentration was assessed by measuring the absorbance at 370 nm using a Perkin-Elmer Lambda 35 UV-vis spectrophotometer, and calculated using a calibration curve for quercetin dissolved in the same media as the dialysate ($R^2 = 0.99695$ over the range between 5 and 30 μg/mL). A control experiment was set up alongside in which the same amount of quercetin was dissolved in DMSO and dialyzed for comparison. This control was set up to eliminate nonspecific adsorption of the drug to the dialysis membrane. The same conditions were used for the three different formulations NC 1, NC 3 and NC 5. To study the serum stability of the same formulations, release studies were repeated in the same way as detailed above except that 1 mL of Wistar rat serum was added to the formulation prior to dialysis obtaining 33.3% final serum concentration.

Shelf Life Stability. Suspensions were sealed in 20 mL glass vials and stored at 4 °C. Three-month stability of NCs dispersions was tested by visual inspection of the physical properties (color and opacity) and also by size and zeta-potential measurements. The measurements were done in triplicate and presented as an average ± SD.

Cell Culture. The HeLa cells cervical-tumor-derived cell line (HeLa; ATCC, CCL-2), the CT26 murine colon carcinoma (CT26; ATCC, CRL-2638), C6 rat glioma (C6; ATCC, CCL-107) and B16F10 (B16F10; ATCC, CRL-6475) were cultured in RPMI media. Human ovarian carcinoma IGROV-1 cell line was obtained from Prof. Iain McNeish (Institute of Cancer Sciences, University of Glasgow, U.K.) and cultured in DMEM media. All media were supplemented with 10% FBS, 50 U/mL penicillin, 50 μg/mL streptomycin, 1% L-glutamine and 1% nonessential amino acids, at 37 °C in 5% CO₂. Cells were routinely grown in 75 cm² canted-neck tissue culture flasks and passaged twice a week using Trypsin/EDTA at 80% confluence.

Cytotoxicity Studies *in Vitro*. Cancerous cell lines were seeded in 96-well plates and incubated with NC suspensions (200 μL of 1–100 μM) in complete media for 48 h. Cytotoxicity was examined by MTT assay. In brief, at the end of the incubation period, media was removed and replaced with 120 μL of MTT solution at a final concentration of 0.5 mg/mL. Cell were incubated for 3 h at 37 °C and 5% CO₂. At the end of the incubation, formazan was dissolved in 200 μL of DMSO and the plate was read at 570 nm in a FLUOstar OPTIMA plate reader (BMG Labtech) and the results were expressed as the percentage cell survival (mean ± SD) and calculated using the following equation: % Cell survival = (A₅₇₀ nm of treated cells/A₅₇₀ nm of untreated control cells) × 100.

Polymerase Chain Reaction (PCR). RNAs were extracted from HeLa and CT26 cell lines according to manufacturer's instructions. Then, 1 μg of RNA per cell line was reverse-transcribed and real-time PCRs were performed in a total volume of 10 μL on a ABI Prism 7500 Fast (Applied Biosciences) PCR System thermal cycler using the following conditions: 40 amplification cycles, denaturation at 95 °C for 15 s and primer annealing and extension at 60 °C for 1 min. PCRs were performed with 50 ng of cDNA in triplicates and no DNA was detectable in samples that did not undergo reverse transcription or in blank runs without cDNA. GAPDH was used as an endogenous control in each cell line.

Fluorescence Labeling of NCs. Fluorescently labeled NCs (drug-free) were prepared for *in vitro* uptake/trafficking and *in vivo* tumor uptake live imaging studies. Dil, emitting in the red region, and DiR, a fluorophore with near-infrared emission, are hydrophobic fluorescent markers which were incorporated into the oil phase at 0.5 wt %/wt (dye/oil) for *in vitro* and *in vivo* studies, respectively. Drug was not encapsulated in such studies to avoid any toxicity related to the drug itself. Formulations were kept protected from light.

Quantification of Fluorescently Labeled NC in HeLa Cells. HeLa cells were incubated with Dil-labeled NC formulations at 10 or 100 μg/mL, for 1 or 4 h in folate free medium and in the presence of excess FA (200 μM). Cells were washed, lysed (1% Triton X-100 in PBS lysis buffer) and centrifuged. Cell lysates were transferred to a 96-well plate. Quantification of the uptake of NCs in cells was carried out against calibration curves prepared by serial dilutions of stock dispersions in the lysis buffer. Fluorescence signals were measured at 590 nm emission using a FLUOstar OPTIMA plate reader (BMG Labtech). The percentage of cellular uptake was calculated as a percentage of the Dil-labeled NC initially added to the cells.

Uptake Studies *in Vitro* by Confocal Laser Scanning Microscopy (CLSM). HeLa cells were seeded on coverslips at a density of 40K cells per a well of a 24-well plate onto glass coverslips. Cells were seeded in folate free RPMI media overnight. Cells were then incubated with 0.5 mL of Dil-labeled NCs 3 (PEGylated, non-FA targeted NC) and NCs 5 (PEGylated, FA-targeted NC). Cells were incubated with either type for 1 or 4 h in folate free medium media. For competitive inhibition of uptake of the FA targeted NC, excess FA was added to the media at a concentration of 200 μM. Optimization of FA concentration was first performed to eliminate toxicity related to high concentrations of FA. At the end of incubation period, cell were rinsed, fixed (200 μL of 4% PFA for 10–15 min at RT), permeabilized (200 μL of 0.1% w/v Triton X-100 for 5 min at RT), and subsequently

incubated with Alexa Fluor 488 phalloidin to stain F-actin (200 μ L of 20 \times dilution of the original stock solution), as directed by the manufacturer; in PBS for 20 min at RT. Coverslips were mounted on glass slides using Mowiol 4-88 mounting media. NCs uptake was represented by the red signals, while cell cytoskeleton was marked in green. Confocal images were captured using a Nikon Eclipse Ti Inverted confocal microscope (Nikon) and images were analyzed by Nikon's NIS element viewer and MacBiophotonics ImageJ.

Animal Studies and Tumor Uptake *in Vivo*. All animal experiments were performed in compliance with the UK Home Office (1989) Code of Practice for the housing and care of Animals used in Scientific Procedures. Female Athymic nude and SHRN mice aged 4–6 weeks (Harlan) were inoculated subcutaneously with HeLa cells (5×10^6 cells in 0.1 mL PBS) or IGROV-1 cells (6×10^{10}) at the lower flanks, respectively. When the tumors reached an appropriate size (600 mm 3), mice were maintained on a folate-free diet (Test Diet) for one week prior to and for the duration of the studies. Mice ($n = 3$) were intravenously injected with as prepared DiR-labeled NC **3** or NC **5** (50 mg polymer/mL, 250 μ L) and scanned at 1, 4, and 24 h post injection using an IVIS Lumina Series III *In Vivo* Imaging System (Perkin-Elmer). Untreated animals were also included as controls. Animals were anesthetized with 1.5% isoflurane/98.5% oxygen to maintain sedation during the imaging procedure. *Ex vivo* imaging was carried out immediately afterward by imaging excised major organs (heart, lung, liver, spleen and kidney) including tumors. Images were quantitatively analyzed by drawing regions of interests around the tissues using Living Image software.

HeLa-bearing mice were injected with DiI-labeled NCs for CLSM studies in which tumors were snap-frozen at 24 h post iv injection. Frozen sections were cut into 8 μ m thick pieces using a cryostat (Bright Instrument Ltd.) and picked up on slides to air-dry at RT. Slides were then kept at -20° C until further use. For CLSM, sections were fixed in 4% PFA at RT for 10–15 min, washed a few times with PBS and then mounted using DAPI containing mounting medium (Vector Laboratories). The intratumoral distribution of NCs was imaged using a Nikon Eclipse Ti Inverted confocal microscope (Nikon) with 561 nm excitation and 570–620 nm emission.

Statistical Analysis. Results were expressed as mean \pm SD. Statistical data analysis was conducted using the graph pad instat software. A comparison of the data was performed using Student's *t* test.

Conflict of Interest: The authors declare no competing financial interest.

Acknowledgment. Funding from missions department, ministry of higher education, Egypt, is greatly acknowledged. The authors would like to thank Prof. Robert Hider (King's College London) for useful discussions on the chemical functionalization of the polymers and Dr. Patrick Mesquida and Mr. William Luckhurst (King's College London) on discussions in interpreting the AFM analysis. Funding from Biotechnology and Biological Sciences Research Council (BB/J008656/1), Associated International Cancer Research (AICR), the EU FP7-ITN Marie-Curie Network programme RADDEL (290023) is acknowledged. H.K. is supported by the Atomic Energy Commission of Syria (AECS). The authors acknowledge financial support from the EU 7FP Program No. 262348 (European Soft Matter Infrastructure, ESMI) and the Belgian government through the Interuniversity Attraction Pole (IAP-PAI).

Note Added after ASAP Publication: This paper published ASAP on January 23, 2014. Figure 8 was replaced and the revised version was reposted on February 3, 2014.

Supporting Information Available: Characterization methods and instrumentation; movies (avi and .mpg) of the set of 2D projection images which is acquired NC **3** sample and volume rendering of a 3D reconstruction of NC **3** showing the nanocapsules in their hydrated state. This material is available free of charge via the Internet at <http://pubs.acs.org>.

REFERENCES AND NOTES

- Mosqueira, V. C. F.; Legrand, P.; Morgat, J. L.; Vert, M.; Myslakine, E.; Gref, R.; Devissaguet, J. P.; Barratt, G. Biodistribution of Long-Circulating PEG-Grafted Nanocapsules in Mice: Effects of PEG Chain Length and Density. *Pharm. Res.* **2001**, *18*, 1411–1419.
- Pereira, M. A.; Mosqueira, V. C. F.; Vilelac, J. M. C.; Andrade, M. S.; Ramaldes, G. A.; Cardoso, V. N. PLA-PEG Nanocapsules Radiolabeled with 99mTechnetium-HMPAO: Release Properties and Physicochemical Characterization by Atomic Force Microscopy and Photon Correlation Spectroscopy. *Eur. J. Pharm. Sci.* **2008**, *33*, 42–51.
- Mora-Huertas, C. E.; Fessi, H.; Elaissari, A. Polymer-Based Nanocapsules for Drug Delivery. *Int. J. Pharm.* **2010**, *385*, 113–142.
- Mosqueira, V. C. F.; Legrand, P.; Gulik, A.; Bourdon, O.; Gref, R.; Labarre, D.; Barratt, G. Relationship Between Complement Activation, Cellular Uptake and Physicochemical Aspects of Novel PEG-Modified Nanocapsules. *Biomaterials* **2001**, *22*, 2967–2979.
- Gref, R.; Luck, M.; Quellec, P.; Marchand, M.; Dellacherie, E.; Harnisch, S.; Blunk, T.; Muller, R. H. 'Stealth' Corona-Core Nanoparticles Surface Modified by Polyethylene Glycol (PEG): Influences of the Corona (PEG Chain Length and Surface Density) and of the Core Composition on Phagocytic Uptake and Plasma Protein Adsorption. *Colloids Surf. B* **2000**, *18*, 301–313.
- Yuan, Z. P.; Chen, L. J.; Fan, L. Y.; Tang, M. H.; Yang, G. L.; Yang, H. S.; Du, X. B.; Wang, G. O.; Yao, W. X.; Zhao, Q. M. Liposomal Quercetin Efficiently Suppresses Growth of Solid Tumors in Murine Models. *Clin. Cancer Res.* **2006**, *12*, 3193–3199.
- Rogerio, A. P.; Dora, C. L.; Andrade, E. L.; Chaves, J. S.; Silva, L. F. C.; Senna, E. L.; Calixto, J. B. Anti-inflammatory Effect of Quercetin-Loaded Microemulsion in the Airways Allergic Inflammatory Model in Mice. *Pharm. Res.* **2010**, *61*, 288–297.
- Wu, T. H.; Yen, F. L.; Lin, L. T.; Tsai, T. R.; Lin, C. C.; Cham, T. M. Preparation, Physicochemical Characterization and Antioxidant Effects of Quercetin Nanoparticles. *Int. J. Pharm.* **2008**, *346*, 160–168.
- Ghosh, A.; Ghosh, D.; Sarkar, S.; Mandal, A. K.; Choudhury, S. T.; Das, N. Anticarcinogenic Activity of Nanoencapsulated Quercetin in Combating Diethylnitrosamine-Induced Hepatocarcinoma in Rats. *Eur. J. Cancer Prev.* **2012**, *21*, 32–41.
- Vijayababu, M. R.; Arunkumar, A.; Kanagaraj, P.; Venkataraman, P.; Krishnamoorthy, G.; Arunakaran, J. Quercetin Downregulates Matrix Metalloproteinases 2 and 9 Proteins Expression in Prostate Cancer Cells (PC-3). *Mol. Cell. Biochem.* **2006**, *287*, 109–116.
- Lang, D. R.; Racker, E. Inhibition of NaK Adenosine Triphosphatase and Its Partial Reactions by Quercetin. *Biochemistry* **1974**, *15*, 4951–4958.
- Hoffmann, J.; Doppler, W.; Jakob, A.; Maly, K.; Posch, L.; Überall, F.; Grunicke, H. H. Enhancement of the Antiproliferative Effects of *cis*-Diamminedichloroplatinum(II) and Nitrogen Mustard by Inhibitors of Protein Kinase C. *Int. J. Cancer* **1988**, *42*, 382–388.
- Srivastava, A. K. Inhibition of Phosphorylase Kinase and Tyrosine Protein Kinase Activities by Quercetin. *Biochem. Biophys. Res. Commun.* **1985**, *131*, 1–5.
- Ferry, D. R.; Smith, A.; Malkhandi, J.; Fyfe, D. W.; DeTakats, P. G.; Anderson, D.; Baker, J.; Kerr, D. J. Phase I Clinical Trial of the Flavonoid Quercetin: Pharmacokinetics and Evidence for *In Vivo* Tyrosine Kinase Inhibition. *Clin. Cancer Res.* **1996**, *2*, 659–668.
- Mulholland, P. J.; Ferry, D. R.; Anderson, D.; Hussain, S. A.; Young, A. M.; Cook, J. E.; Hodgkin, E.; Seymour, L. W.; Kerr, D. J. Pre-Clinical and Clinical Study of OC12, a Water-Soluble, Pro-Drug of Quercetin. *Ann. Oncol.* **2001**, *12*, 245–248.
- Kale, R.; Saraf, M.; Juvekar, A.; Tayade, P. Decreased B16F10 Melanoma Growth and Impaired Tumour Vascularization in BDF1Mice with Quercetin–Cyclodextrin Binary System. *J. Pharm. Pharmacol.* **2006**, *58*, 1351–1358.
- Yadav, A. V.; Murthy, M. S.; Shete, A. S.; Sakhar, S. Stability Aspects of Liposomes. *Indian J. Pharm. Educ. Res.* **2011**, *45*, 402–413.
- Esmaili, F.; Ghahremani, M. H.; Ostad, S. N.; Atyabi, F.; Seyedarabi, M.; Maleekshahi, M. R.; Amini, M.; Dinarvand, S.

R. Folate-Receptor-Targeted Delivery of Docetaxel Nanoparticles Prepared by PLGA-PEG-Folate Conjugate. *J. Drug Targeting* **2008**, *16*, 415–423.

19. Yoo, H. S.; Park, T. G. Folate Receptor Targeted Biodegradable Polymeric Doxorubicin Micelles. *J. Controlled Release* **2004**, *96*, 273–283.

20. Boddu, S. H. S.; Vaishya, R.; Jwala, J.; Vadlapudi, A.; Pal, D.; Mitra, A. K. Preparation and Characterization of Folate Conjugated Nanoparticles of Doxorubicin Using PLGA-PEG-FOL Polymer. *Med. Chem.* **2012**, *2*, 068–075.

21. Liu, F.; Deng, D.; Chen, X.; Qian, Z.; Achilefu, S.; Gu, Y. Folate-Polyethylene Glycol Conjugated Near-Infrared Fluorescence Probe with High Targeting Affinity and Sensitivity for *In Vivo* Early Tumor Diagnosis. *Mol. Imaging Biol.* **2010**, *12*, 595–607.

22. Kaiser, E.; Colescott, R. L.; Bossinge, C. D.; Cook, P. I. Color Test for Detection of Free Terminal Amino Groups in Solid-Phase Synthesis of Peptides. *Anal. Biochem.* **1970**, *34*, 595–598.

23. Sarin, V. K.; Kent, S. B. H.; Tam, J. P.; Merrifield, R. B. Quantitative Monitoring of Solid-Phase Peptide Synthesis by the Ninhydrin Reaction. *Anal. Biochem.* **1981**, *117*, 147–157.

24. Sims, G. E. C.; Snape, T. J. A Method for the Estimation of Polyethylene Glycol in Plasma Protein Fraction. *Anal. Biochem.* **1980**, *107*, 60–63.

25. Chung, T. W.; Chung, C. H.; Lue, W. F. A. A Colorimetric Method for Determining Distearylphosphatidylethanolamine-Polyethylene Glycol 2000 in Blood Suspension. *Anal. Biochem.* **2000**, *285*, 264–267.

26. Fessi, H.; Puisieux, F.; Devissaguet, J.; Ammoury, N.; Benita, S. Nanocapsule Formation by Interfacial Polymer Deposition Following Solvent Displacement. *Int. J. Pharm.* **1989**, *55*, R1–R4.

27. Neckel, G. L.; Nemen, D.; Puhl, A. C.; Fernandes, D.; Stiampaglio, M. A.; Silva, M. A.; Hangai, M.; Silva, M. C. S.; Senna, E. L. Stealth and Non-Stealth Nanocapsules Containing Camptothecin: *In Vitro* and *In Vivo* Activity on B16-F10 Melanoma. *J. Pharm. Pharmacol.* **2007**, *59*, 1359–1364.

28. Li, Y. P.; Pei, Y. Y.; Zhang, X. Y.; Gu, Z. H.; Zhou, Z. H.; Yuan, W. F.; Zhou, J. J.; Zhu, J. H.; Gao, X. J. PEGylated PLGA Nanoparticles as Protein Carriers: Synthesis, Preparation and Biodistribution in Rats. *J. Controlled Release* **2001**, *71*, 203–211.

29. Anand, P.; Nair, H. B.; Sung, B.; Kunnumakkara, A. B.; Yadav, V. R.; Tekmal, R. R.; Aggarwal, B. B. Design of Curcumin-Loaded PLGA Nanoparticles Formulation with Enhanced Cellular Uptake and Increased Bioactivity *In Vitro* and Superior Bioavailability *In Vitro*. *Biochem. Pharmacol.* **2010**, *79*, 330–338.

30. Mansoori, G. A.; Brandenburg, K. S.; Zadeh, A. S. A. Comparative Study of Two Folate-Conjugated Gold Nanoparticles for Cancer Nanotechnology Applications. *Cancers* **2010**, *2*, 1911–1928.

31. Lu, T.; Sun, S.; Chen, X.; Zhang, P.; Jing, X. Folate-Conjugated Micelles and Their Folate-Receptor-Mediated Endocytosis. *Macromol. Biosci.* **2009**, *9*, 1059–1068.

32. Nie, Y.; Zhang, Z.; Li, L.; Luo, K.; Ding, H.; Gu, Z. Synthesis, Characterization and Transfection of a Novel Folate Targeted Multipolymeric Nanoparticles for Gene Delivery. *J. Mater. Sci.: Mater. Med.* **2009**, *20*, 1849–1857.

33. Bose, S.; Du, Y.; Takhistov, P.; Michniak-Kohn, B. Formulation, Optimization and Topical Delivery of Quercetin from Solid Lipid Based Nanosystems. *Int. J. Pharm.* **2013**, *441*, 56–66.

34. Dhawan, S.; Kapil, R.; Singh, B. Formulation, Development and Systematic Optimization of Solid Lipid Nanoparticles of Quercetin for Improved Brain Delivery. *J. Pharm. Pharmacol.* **2011**, *63*, 342–351.

35. Vicentini, F. T. M. C.; Simi, T. R. M.; Del Ciampo, J. O.; Wolga, N. O.; Pitol, D. L.; Iyomasa, M. M.; Bentley, M. V. L. B.; Fonseca, M. J. V. Quercetin in W/O Microemulsion: *In Vitro* and *In Vivo* Skin Penetration and Efficacy against UVB-Induced Skin Damages Evaluated *In Vivo*. *Eur. J. Pharm. Biopharm.* **2008**, *69*, 948–957.

36. Das, S.; Mandal, A. K.; Ghosh, A.; Panda, S.; Das, N.; Sarkar, S. Nanoparticulated Quercetin in Combating Age Related Cerebral Oxidative Injury. *Curr. Aging Sci.* **2008**, *1*, 169–174.

37. Kumari, A.; Yadav, S. K.; Pakade, Y. B.; Singh, B.; Yadav, S. C. Development of Biodegradable Nanoparticles for Delivery of Quercetin. *Colloids Surf., B* **2010**, *80*, 184–192.

38. Ghosh, A.; Mandal, A. K.; Sarkar, S.; Panda, S.; Das, N. Nanoencapsulation of Quercetin Enhances Its Dietary Efficacy in Combating Arsenic-Induced Oxidative Damage in Liver and Brain of Rats. *Life Sci.* **2009**, *84*, 75–80.

39. Kumari, A.; Kumar, V.; Yadav, S. K. Plant Extract Synthesized PLA Nanoparticles for Controlled and Sustained Release of Quercetin: A Green Approach. *PLoS One* **2012**, *7*, 1–10.

40. Weiss-Angeli, V.; Poletto, F. S.; de Marco, S. L.; Salvador, M.; da Silveira, N. P.; Guterres; Pohlmann, A. R. Sustained Antioxidant Activity of Quercetin-Loaded Lipid-Core Nanocapsules. *J. Nanosci. Nanotechnol.* **2012**, *12*, 2874–2880.

41. Gang, W.; Jie, W. J.; Ping, Z. L.; Ming, D. S.; Ying, L. J.; Lei, W.; Fang, Y. Liposomal Quercetin: Evaluating Drug Delivery *In Vitro* and Biodistribution *In Vivo*. *Expert Opin. Drug Delivery* **2012**, *9*, 599–613.

42. Wang, Q.; Bao, Y.; Ahire, J.; Chao, Y. Co-Encapsulation of Biodegradable Nanoparticles with Silicon Quantum Dots and Quercetin for Monitored Delivery. *Adv. Healthcare Mater.* **2013**, *2*, 459–466.

43. Wang, G.; Wang, J. J.; Luo, J.; Wang, L.; Chen, X. L.; Zhang, L. P.; Jiang, S. Q. PEG2000-DPSE-Coated Quercetin Nanoparticles Remarkably Enhanced Anticancer Effects through Induced Programed Cell Death on C6 Glioma Cells. *J. Biomed. Mater. Res., Part A* **2013**, *101*, 3076–3085.

44. Sheng, Y.; Yuan, Y.; Liu, C. S.; Tao, X.; Shan, X.; Xu, F. *In Vitro* Macrophage Uptake and *In Vivo* Biodistribution of PLA-PEG Nanoparticles Loaded with Hemoglobin as Blood Substitutes: Effect of PEG Content. *J. Mater. Sci.: Mater. Med.* **2009**, *20*, 1881–1891.

45. Ameller, T.; Marsaud, V.; Legrand, P.; Gref, R.; Barratt, G.; Renoir, J. M. Polyester Poly (Ethylene Glycol) Nanoparticles Loaded with the Pure Antiestrogen RU 58668: Physicochemical and Opsonization Properties. *Pharm. Res.* **2003**, *20*, 1063–1070.

46. Leite, E. A.; Vilela, J. M. C.; Mosqueira, V. C. F.; Andrade, M. S. Poly-Caprolactone Nanocapsules Morphological Features by Atomic Force Microscopy. *Microsc. Microanal.* **2005**, *11*, 48–51.

47. Kuntsche, J.; Horstb, J. C.; Bunjesb, H. Cryogenic Transmission Electron Microscopy (Cryo-TEM) for Studying Thiomorphology of Colloidal Drug Delivery Systems. *Int. J. Pharm.* **2011**, *417*, 120–137.

48. Mosqueira, V. C. F.; Legrand, P.; Pinto-Alphandary, H.; Puisieux, F.; Barratt, G. Poly(D,L-Lactide) Nanocapsules Prepared by A Solvent Displacement Process: Influence of the Composition on Physicochemical and Structural Properties. *J. Pharm. Sci.* **2000**, *89*, 614–625.

49. Barras, A.; Mezzetti, A.; Richarda, A.; Lazzaronib, S.; Rouxa, S.; Melnyka, P.; Betbederd, D.; Monfilliette-Dupont, N. Formulation and Characterization of Polyphenol-Loaded Lipid Nanocapsules. *Int. J. Pharm.* **2009**, *379*, 270–277.

50. Cauchetier, E.; Deniau, M.; Fessi, H.; Astier, A.; Paul, M. Atovaquone-Loaded Nanocapsules: Influence of the Nature of the Polymer on Their *In Vitro* Characteristics. *Int. J. Pharm.* **2003**, *250*, 273–281.

51. Mosqueira, V. C. F.; Legrand, P.; Barratt, G. Surface-Modified and Conventional Nanocapsules as Novel Formulations for Parenteral Delivery of Halofantrine. *J. Nanosci. Nanotechnol.* **2006**, *6*, 3193–3202.

52. Priyadarsini, R. V.; Murugan, R. S.; Maitreyi, S.; Ramalingam, K.; Karunagaran, D.; Nagini, S. The Flavonoid Quercetin Induces Cell Cycle Arrest and Mitochondria-Mediated Apoptosis in Human Cervical Cancer (HeLa) Cells through p53 Induction and NF- κ B Inhibition. *Eur. J. Pharmacol.* **2010**, *649*, 84–91.

53. Goniotaki, M.; Hatziantoniou, S.; Dimas, K.; Wagner, M.; Demetzos, C. Encapsulation of Naturally Occurring Flavonoids into Liposomes: Physicochemical Properties and Biological Activity Against Human Cancer Cell Lines. *J. Pharm. Pharmacol.* **2004**, *56*, 1217–1224.
54. Petersen, S.; Fahr, A.; Bunjes, H. Flow Cytometry as a New Approach To Investigate Drug Transfer between Lipid Particles. *Mol. Pharmaceutics* **2010**, *7*, 350–363.
55. Gabizon, A.; Horowitz, A. T.; Goren, D.; Tzemach, D.; Shmeeda, H.; Zalipsky, S. *In Vivo* Fate of Folate-Targeted Polyethylene-Glycol Liposomes in Tumor-Bearing Mice. *Clin. Cancer Res.* **2003**, *9*, 6551–6559.
56. Xiang, G.; Wu, J.; Lu, Y.; Liu, Z.; Lee, R. J. Synthesis and Evaluation of a Novel Ligand for Folate-Mediated Targeting Liposomes. *Int. J. Pharm.* **2008**, *356*, 29–36.
57. Liang, C.; Yang, C.; Ling, Y.; Huang, Y.; Li, T.; Li, X. Improved Therapeutic Effect of Folate-Decorated PLGA–PEG Nanoparticles for Endometrial Carcinoma. *Bioorg. Med. Chem.* **2011**, *19*, 4057–4066.
58. Bharali, D. J.; Siddiqui, I. A.; Adhami, V. M.; Chamcheu, J. C.; Aldahmash, A. M.; Mukhtar, M.; Mousa, S. A. Nanoparticle Delivery of Natural Products in the Prevention and Treatment of Cancers: Current Status and Future Prospects. *Cancers* **2011**, *3*, 4024–4045.
59. Blanco, M. D.; Guerrero, S.; Benito, M.; Fernández, A.; Teijón, C.; Olmo, R.; Katime, I.; Teijón, J. M. *In Vitro* and *in Vivo* Evaluation of a Folate-Targeted Copolymeric Submicrohydrogel Based on N-Isopropylacrylamide as 5-Fluorouracil Delivery System. *Polymers* **2011**, *3*, 1107–1125.
60. Rata-Aguilar, A.; Sánchez-Moreno, P.; Jódar-Reyes, A. B.; Martín-Rodríguez, A.; Boulai, H.; Marchal-Corrales, J. A.; Peula-García, J. M.; Ortega-Vinuesa, J. L. Colloidal Stability and *“in Vitro”* Antitumor Targeting Ability of Lipid Nanocapsules Coated by Folate-Chitosan Conjugates. *J. Bioact. Compat. Polym.* **2012**, *27*, 388–404.